Copyright Warning & Restrictions

The copyright law of the United States (Title 17, United States Code) governs the making of photocopies or other reproductions of copyrighted material.

Under certain conditions specified in the law, libraries and archives are authorized to furnish a photocopy or other reproduction. One of these specified conditions is that the photocopy or reproduction is not to be "used for any purpose other than private study, scholarship, or research." If a, user makes a request for, or later uses, a photocopy or reproduction for purposes in excess of "fair use" that user may be liable for copyright infringement,

This institution reserves the right to refuse to accept a copying order if, in its judgment, fulfillment of the order would involve violation of copyright law.

Please Note: The author retains the copyright while the New Jersey Institute of Technology reserves the right to distribute this thesis or dissertation

Printing note: If you do not wish to print this page, then select "Pages from: first page # to: last page #" on the print dialog screen

ABSTRACT

DUAL-BATTERY EMPOWERED GREEN CELLULAR NETWORKS

by
Xilong Liu

With awareness of the potential harmful effects to the environment and climate change, on-grid brown energy consumption of information and communications technology (ICT) has drawn much attention. Cellular base stations (BSs) are among the major energy guzzlers in ICT, and their contributions to the global carbon emissions increase sustainedly. It is essential to leverage green energy to power BSs to reduce their on-grid brown energy consumption. However, in order to furthest save on-grid brown energy and decrease the on-grid brown energy electricity expenses, most existing green energy related works only pursue to maximize the green energy utilization while compromising the services received by the mobile users. In reality, dissatisfaction of services may eventually lead to loss of market shares and profits of the network providers. In this research, a dual-battery enabled profit driven user association scheme is introduced to jointly consider the traffic delivery latency and green energy utilization to maximize the profits for the network providers in heterogeneous cellular networks. Since this profit driven user association optimization problem is NP-hard, some heuristics are presented to solve the problem with low computational complexity. Finally, the performance of the proposed algorithm is validated through extensive simulations.

In addition, the Internet of Things (IoT) heralds a vision of future Internet where all physical things/devices are connected via a network to promote a heightened level of awareness about our world and dramatically improve our daily lives. Nonetheless, most wireless technologies utilizing unlicensed bands cannot provision ubiquitous and quality IoT services. In contrast, cellular networks support large-scale, quality of service guaranteed, and secured communications. However, tremendous

proximal communications via local BSs will lead to severe traffic congestion and huge energy consumption in conventional cellular networks. Device-to-device (D2D) communications can potentially offload traffic from and reduce energy consumption of BSs. In order to realize the vision of a truly global IoT, a novel architecture, i.e., overlay-based green relay assisted D2D communications with dual batteries in heterogeneous cellular networks, is introduced. By optimally allocating the network resource, the introduced resource allocation method provisions the IoT services and minimizes the overall energy consumption of the pico relay BSs. By balancing the residual green energy among the pico relay BSs, the green energy utilization is maximized; this furthest saves the on-grid energy. Finally, the performance of the proposed architecture is validated through extensive simulations.

Furthermore, the mobile devices serve the important roles in cellular networks and IoT. With the ongoing worldwide development of IoT, an unprecedented number of edge devices imperatively consume a substantial amount of energy. The overall IoT mobile edge devices have been predicted to be the leading energy guzzler in ICT by 2020. Therefore, a three-step green IoT architecture is proposed, i.e., ambient energy harvesting, green energy wireless transfer and green energy balancing, in this research. The latter step reinforces the former one to ensure the availability of green energy. The basic design principles for these three steps are laid out and discussed.

In summary, based on the dual-battery architecture, this dissertation research proposes solutions for the three aspects, i.e., green cellular BSs, green D2D communications and green devices, to hopefully and eventually actualize green cellular access networks, as part of the ongoing efforts in greening our society and environment.

DUAL-BATTERY EMPOWERED GREEN CELLULAR NETWORKS

by
Xilong Liu

A Dissertation
Submitted to the Faculty of
New Jersey Institute of Technology
in Partial Fulfillment of the Requirements for the Degree of
Doctor of Philosophy in Electrical Engineering

Helen and John C. Hartmann Department of
Electrical and Computer Engineering

May 2019

APPROVAL PAGE

DUAL-BATTERY EMPOWERED GREEN CELLULAR NETWORKS

Xilong Liu

Dr. Nirwan Ansari, Dissertation Advisor — Date
Distinguished Professor, Department of Electrical and Computer Engineering, NJIT

Dr. Cristian Borcea, Committee Member — Date
Professor, Department of Computer Science, NJIT

Dr. Abdallah Khreishah, Committee Member — Date
Associate Professor, Department of Electrical and Computer Engineering, NJIT

Dr. Roberto Rojas-Cessa, Committee Member — Date
Professor, Department of Electrical and Computer Engineering, NJIT

Dr. Mengchu Zhou, Committee Member — Date
Distinguished Professor, Department of Electrical and Computer Engineering, NJIT

BIOGRAPHICAL SKETCH

Author: Xilong Liu

Degree: Doctor of Philosophy

Date: May 2019

Undergraduate and Graduate Education:

- Doctor of Philosophy in Electrical Engineering,
  New Jersey Institute of Technology, Newark, NJ, 2019
- Master of Science in Electrical Engineering,
  New Jersey Institute of Technology, Newark, NJ, 2013
- Bachelor of Engineering in Telecommunication,
  Zhengzhou University, Henan, P.R.China, 2011

Major: Electrical Engineering

Presentations and Publications:

Book chapter:

X. Liu and N. Ansari, "Energy-Efficient/Green Design for D2D," *Wiley 5G Ref*, 2019. (Submitted)

Journal articles:

X. Liu and N. Ansari, "Toward Green IoT: Energy Solutions and Key Challenges," *IEEE Communications Magazine*, vol. 57, no. 3, pp. 104-110, Mar. 2019.

X. Liu and N. Ansari, "Resource Allocation in UAV-assisted M2M Communications for Disaster Rescue," *IEEE Wireless Communications Letters*, vol. 8 , no. 2, pp. 580-583, Apr. 2019.

X. Liu and N. Ansari, "Dual-Battery Enabled Profit Driven User Association in Green Heterogeneous Cellular Networks," *IEEE Transactions on Green Communications and Networking*, vol. 2, no. 4, pp. 1002-1011, Dec. 2018.

X. Liu and N. Ansari, "Green Relay Assisted D2D Communications with Dual Batteries in Heterogeneous Cellular Networks for IoT," *IEEE Internet of Things Journal*, vol. 4, no. 5, pp. 1707–1715, Oct. 2017.

X. Liu and N. Ansari, "Profit-driven User Association and Smart Grid Energy Transfer in Green Cellular Networks," *IEEE Transactions on Vehicular Technology*, 2019. (Submitted)

Conference papers:

X. Liu and N. Ansari, "Dual-Battery Enabled Green Proximal M2M Communications in LPWA for IoT," *IEEE International Conference on Communications (ICC)*, Kansas City, 2018.

X. Liu and N. Ansari, "Profit Driven User Association with Dual Batteries in Green Heterogeneous Cellular Networks," *IEEE Global Communications Conference (GLOBECOM)*, Singapore, 2017.

X. Liu and N. Ansari, "Green Relay Assisted D2D Communications with Dual Battery for IoT," *IEEE Global Communications Conference (GLOBECOM)*, Washington D.C., 2016.

X. Liu, X. Huang and N. Ansari, "Green Energy Driven User Association in Cellular Networks with Dual Battery System," *IEEE International Conference on Communications (ICC)*, Kuala Lumpur, 2016.

X. Liu, T. Han and N. Ansari, "Intelligent Battery Management for Cellular Networks with Hybrid Energy Supplies," *IEEE Wireless Communications and Networking Conference (WCNC)*, Doha, 2016.

Once a prince, always a prince.

ACKNOWLEDGMENT

My deepest gratitude is to my dear advisor, Dr. Nirwan Ansari. I have been amazingly fortunate to have him in my doctoral studies. His persistent guidance, support and encouragement helped me overcome many difficult situations throughout my research and life. Without his continuous help, this dissertation would not have been possible.

To my committee members, Dr. Cristian Borcea, Dr. Abdallah Khreishah, Dr. Roberto Rojas-Cessa, and Dr. Mengchu Zhou. I thank them for their time and advisement.

I would like to thank U.S. Nation Science Foundation (NSF) for the funding support in my research. I would like to extend my gratitude to other faculty and staff members of our Department of Electrical and Computer Engineering for their support throughout my doctoral studies. I also want to thank my good friends: Yan Zhang, Tao Han, Mina Taheri, Xueqing Huang, Xiang Sun, Abbas Kiani, Qiang Fan, Ali Shahini, Liang Zhang, Di Wu, Jingjing Yao, Shuai Zhang, Weiqi Liu, Weiqiang Dong, Xiaoyu Lu, Jingchu Ji, Jianchen Shan, Xin Gao, and many others, who have given me strength and encouragement over the last five years. I would like to thank my parents and family for their years' support. I would like to express appreciation to my girlfriend, Xiao Yang, for her care and understanding.

TABLE OF CONTENTS

TABLE OF CONTENTS
(Continued)

Chapter **Page**

LIST OF TABLES

Table **Page**

LIST OF FIGURES

LIST OF FIGURES
(Continued)

Figure **Page**

CHAPTER 1

INTRODUCTION

With awareness of the potential harmful effects to the environment and climate change caused by carbon footprints and considering the depletion of brown energy sources, much attention has been drawn from the society to reduce the usage of brown energy. It is reported that by 2020, average annual Information and Communication Technology (ICT) carbon emissions contribution will be 6%-8% [55]. Cellular networks account for more than 10% of ICT carbon emissions and base stations (BSs) consume more than 50% total energy in cellular networks [51], [23]. Therefore, it is crucial and urgent to reduce the on-grid brown energy consumption of BSs in cellular networks.

Ericsson has designed a wind-powered tower for BSs in cellular networks [5]. Nokia Siemens Networks has developed a green BS powered by solar and wind power to reduce the grid electricity consumption. Powering BSs with green energy can effectively reduce on-grid energy and CO_2 footprints of cellular networks.

From the perspective of cellular networks providers, reducing on-grid energy consumption is not only a matter of assuming environmental responsibility, but also of substantially decreasing their operational expenditure (OPEX) [40]. It is estimated that more than 10 billion dollars are spent by cellular network providers for electricity per year, which is a significant portion of the OPEX [51]. As green energy technologies advance, it is promising to leverage green energy, such as solar and wind energy [44], to power BSs. Powering BSs with green energy can effectively reduce carbon footprints and save on-grid electricity expenses.

Since both green energy generations and communication workloads at individual BSs exhibit temporal and spatial diversities, the mismatch between the amount of

available green energy and that of workload demanded energy leads to poor utilization of green energy. Therefore, to furthest reduce the on-grid energy consumption, maximizing the utilization of green energy has become a well pursued research topic [8].

To maximize green energy utilization, the first significant step is to be aware of the amount of available green energy in the network. However, most existing green energy related works simply assume that the generation rate of green energy can be perfectly predicted [23], [28]. In fact, it is difficult to predict the available green energy or green energy generation rate in advance because green energy generation depends on plenty of natural and human factors. Even though some weather prediction models have been introduced, for particular BSs, they are grossly inaccurate in reality [44], [39]. Inaccuracy will lead to the green energy wastage and network performance degradation.

In this research, the dual-battery architecture is invented to harvest, store and utilize green energy. First, by installing dual-battery at each BS, there is no need to predict the available green energy; the amount of harvested green energy in the battery is known and accurate. Second, dual-battery enables the BS with concurrent green energy harvesting and BS powering, i.e., one battery is for charging, the other one discharges to power BS, and they alternate their roles of charging and discharging every time period. Third, without energy storage, instantaneously available green energy from environment at a BS may not be sufficient to perform effective transmission; by adopting dual-battery, the harvested green energy can be stored and accumulated to a certain energy level during the time period.

Intuitively, in order to maximize green energy utilization and reduce on-gird electricity expenses, most related works propose user-BS association schemes to associate more mobile users to the BSs, which have more abundant green energy [44]. This is seemingly rational, but brings potential negative effects. First, disassociating

mobile users from the original nearest BS and associating them to other far away BSs will incur more overall transmission energy consumption to serve these users due to the wireless propagation attenuation. Second, associating a large number of users to a particular BS at once may also lead to heavy traffic congestion and high traffic delivery latency. Degraded quality of service (QoS) leads to dissatisfaction on user experience that will eventually lose customers and profits [28].

Taking into account of these issues comprehensively, in Chapter 2, the dual-battery enabled profit driven user association scheme is presented to jointly consider the green energy utilization and traffic delivery latency in a heterogeneous cellular network. Since this profit driven user association optimization problem is NP-hard, a heuristic algorithm is proposed to maximize the total profit with low computational complexity.

In addition, Internet of Things (IoT) recently heralds a vision of future Internet where all the physical things are connected through a network to exchange information about themselves and their surroundings. IoT promotes a heightened level of awareness about our world and bestows intelligence in our daily lives. Physical things are embedded with electronics, software, sensing ability and network connectivity, and are thus enabled to gather, share, forward information and collaborate with each other. Examples of such things can be sensors, health care gadgets, mobile phones, smart meters, home appliances, and even smart furnitures and vehicles. In general, all these featured things are referred to as devices. IoT can enrich our lives and improve our daily experience by providing a platform for connecting all the possible devices cooperatively [38].

Wireless solutions to realizing IoT are critical owing to pervasiveness of emerging mobile IoT devices. However, most wireless technologies, which utilize unlicensed bands, cannot provision the ubiquitous, seamless and quality service required for IoT. For instance, Zigbee only enables low data rate transmission, and single channel

incurs dense interference; Bluetooth is limited to short range transmission and is sensitive to fading and interference; Low Power Wide Area (LPWA) only allows low data rate transmission and is sensitive to fading as well, and lacks scalability for large-scale IoT [4]; WiFi suffers from poor mobility and roaming support, and does not offer guaranteed quality of services (QoS), due to high interference caused by sharing the unlicensed 2.4 GHz band with Zigbee, Bluetooth, and many other unlicensed band technologies [52]. As compared to unlicensed band technologies, cellular networks provide global coverage, resource management and QoS guaranteed and secured services, as well as mobility and roaming support.

Stimulated by the emerging IoT market, the cellular providers are introducing IoT functionalities into their networks [60], [35]. However, a large number of proximal devices communicating through a local base station (BS) in a conventional cellular network will incur severe traffic congestion, high latency, and huge energy consumption at BS. Therefore, Device-to-Device (D2D) communications has received much attention in cellular networks [60], in which the source and destination devices can directly communicate with minimal assistance from BS, thus providing multiple performance benefits. First, due to the short range communications, proximal D2D devices can enjoy high data rates with low end-to-end delay and low energy consumption. Second, it is more resource-efficient for proximal devices to communicate directly than routing through an involved BS and possibly core network [35]. Third, direct path offloads cellular traffic in BSs and network, thus alleviating congestion, and consequently benefiting other non-D2D users as well [35].

In Chapter 3, the green device-to-device (D2D) communications is investigated. In order to improve spectrum efficiency, existing D2D communications leverages the underlay spectrum sharing approach in a homogeneous cellular network. In this sharing approach, D2D transmissions reuse the spectrum of the cellular network, and are thus subject to the interference caused by the cellular users; inversely, the cellular

communications can also be interfered by D2D users. Many works have been proposed to alleviate this interference issue. However, most of their bandwidth allocation and power control problems are NP-hard. Although some heuristics have been proposed to reduce the runtime, the interference still cannot be eliminated [36]. These works are only tenable with dozens of active D2D devices in a macrocell. When the number of D2D devices increases to realize the large-scale and ubiquitous IoT, the mutual interference is insurmountable. In addition, in their underlay schemes, cellular users are served with high priority [67], while D2D services are not guaranteed.

By taking into account of all these issues comprehensively, in order to actualize the vision of a truly global IoT, in Chapter 3, a novel architecture, i.e., overlay based green relay assisted Device-to-Device communications with dual-battery is discussed and implemented in heterogeneous cellular networks for IoT. By leveraging existing cellular infrastructure, the low power pico BSs act as the relay BSs to facilitate D2D communications. IoT devices are assumed to be driven by the unified D2D communications protocol. By optimally allocating the network resource, the mentioned resource allocation method fulfills the required IoT service data rates and minimizes the overall energy consumption of the relay BSs. To supplement energy provisioning, the relay BSs are equipped with solar panels and dual-batteries to harvest and utilize green energy. Also, the relay BSs are connected by networking cables/fibers and electric transmission lines, for sharing the D2D routing information and maximizing the green energy utilization, respectively.

Chapter 4 focuses on the green devices in IoT. IoT is empowering an intelligent infrastructure, in which uniquely identifiable physical objects are capable of wirelessly communicating with each other to find the state of interests, take proper actions, and gain intelligence from the network. IoT promotes a heightened level of awareness about our world and makes our life more intelligent, efficient and convenient. Examples of such things include smartphones, sensors, health care gadgets, smart

meters, home appliances, and even smart furnitures and vehicles. In general, all these featured things are referred to as IoT devices. It is predicted that more than 50 billion IoT devices will be connected by 2020 in expanding IoT.

In this study, three steps are holistically envisioned to revolutionize and actualize green IoT. First, IoT devices leverage green energy harvesting techniques to harvest "free" energy from ambient energy sources to support their IoT functionalities. When the available ambient green energy in the first step is insufficient to power IoT devices, in the second step, nearby green femto base stations (FBSs) and green pico base stations (PBSs) will intentionally wirelessly transfer green energy to power IoT devices. These green FBSs/PBSs are equipped with solar panels and/or wind turbines and batteries to harvest and store solar and/or wind energy, and then to wirelessy charge IoT devices. As both the amount of harvested green energy and that to be wirelessly transferred at individual FBSs/PBSs exhibit temporal and spatial diversities, the third step is to balance green energy among the FBSs/PBSs to allow more IoT devices to leverage green energy. The latter step reinforces the former one to ensure the availability of green energy.

The rest of this research thesis is organized as follows. In Chapter 2, dual-battery enabled green cellular BSs and profit driven user association scheme are discussed and investigated. In Chapter 3, the green D2D communications is designed and illustrated. Chapter 4 presents the energy solution and key challenges in greening IoT edge devices. Future work is introduced in Chapter 5. Concluding remarks are highlighted in Chapter 6.

CHAPTER 2

GREEN CELLULAR BASE STATIONS

As aforementioned, as cellular bases stations (BSs) consume a huge amount of energy in ICT, it is promising to utilize green energy to power the cellular BSs. Since both green energy generations and communication workloads at individual BSs exhibit temporal and spatial diversities, the mismatch between the amount of available green energy and that of workload demanded energy leads to poor utilization of green energy. Therefore, to furthest reduce the on-grid energy consumption, maximizing the utilization of green energy has become a well pursued research topic [8]. To maximize green energy utilization, the first significant step is to be aware of the amount of available green energy in the network.

2.1 Markov Decision Process Intelligent Battery Management Scheme

In this research (the detail information can be referred to [43]), we first borrow the idea from Markov Decision Process (MDP) to predict the solar energy and decide the action of battery in the current time slot. An intelligent battery management mechanism for BSs is implemented to optimize the green energy utilization. MDP is suitable for solving sequential decision making and control problems. Markov chains are built to model the available solar energy and BS workload demands for each time slot, based on the historical data of solar radiation and workload demands at individual BSs. According to the MDP optimal policy iteration algorithm, the optimal battery management strategy is derived in individual time slots. By managing the battery, we can regulate the renewable energy usage in individual time slots, and thus enhance the utilization of renewable energy. However, owing to the dynamics of solar radiation and BS workload demands, a large number of states are required to model the system.

2.1.1 System Model and Problem Formulation

In this research, we investigate how the solar energy and energy storage interact in an individual BS, and how to use Markov chain to represent the solar radiation levels and BS workload conditions. The energy system configuration of BS, as shown in Figure 2.1, can be tailored from a residential solar energy system.

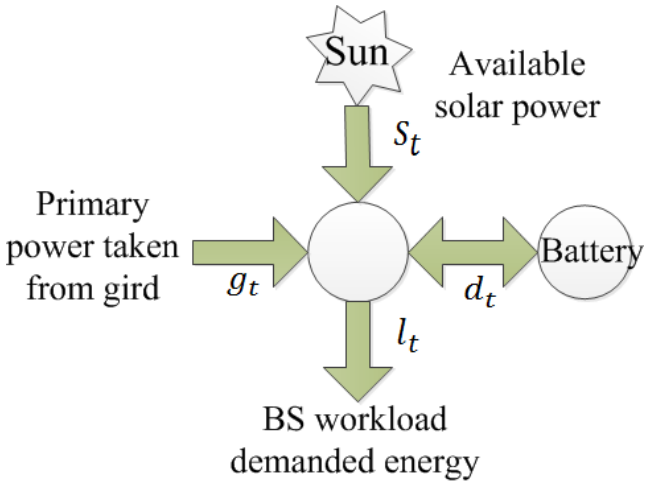

Figure 2.1 General configuration of a base station energy system with battery.

In the system, the time horizon is divided into multiple time slots. We denote s_t, g_t, l_t and d_t as the solar energy, primary power taken from the grid, workload demanded energy in BS, and battery action in each time slot t, respectively.

The connected components of the energy system should achieve energy equilibrium, i.e.,

$$g_t + s_t - l_t - d_t = 0, \tag{2.1}$$

where $d_t \in [-D_{max}, D_{max}]$. The battery converting rate is D_{max}, i.e., in each time slot, the battery is at most charged and discharged of D_{max} and $-D_{max}$ of energy, respectively. A positive d_t refers to the battery charging, a negative d_t implies the battery discharging, and zero means battery being idle. The current battery state is $b_t \in [0, B]$, where B is the battery capacity and $b_{t+1} - b_t = d_{t+1}$.

In this research, we assume that the next 24 hours' electricity prices can be obtained in advance [31] as the day-ahead hourly electricity price is known from utility companies' websites [14]. At each time slot t, the electricity price is denoted as $a_t \in A$.

A Markov chain is a random process that undergoes transitions from one state to another in a state space. It is usually characterized as "memoryless", implying that the probability of visiting the next state depends only on the current state and not on the sequence of preceding events [29]. Some researchers [26], [70] utilized Markov chains to model the weather condition and the solar radiation, in which they claimed that the next (weather) state depends only on the current state, not on the past few periods of the weather states. According to the historical meteorological raw data, we first quantize the available solar energy into energy states (enumerated by non-negative integers). Suppose the solar energy radiation in time slot t is s^*, the quantized value is calculated as $s_t = \lfloor \frac{s^*}{\Delta_s} \rfloor$. Here, Δ_s is a constant quantization interval. Second, for each time slot, we build a Markov chain. We collect the statistics of the quantized data, and obtain the transition probability between two possible states in every two successive time slots. For example, we first define the time slot to be an hour in this work and the time 7 A.M. has M states in total. For State 1, we collect the statistics and obtain the probabilities $p_{1,1}^{s(7)}, p_{1,2}^{s(7)}, ..., p_{1,M}^{s(7)}$, where $s(7)$ stands for states that can be taken at 7 A.M. So, $p_{1,j}^{s(7)}$, $j \in \{1, 2, ..., M\}$, is the probability of transiting from State 1 at 7 A.M. to State j in the next time slot, that is, 8 A.M.. Determining the transition probability matrix will be detailed later on. The solar transition probability from the ith state to the jth state is represented as $p_{i,j}^{s}$. Each time slot has its own transition probability matrix $p_{i,j}^{s(t)}$.

According to the historical records of user traffic at individual BSs, we can obtain the BS workload energy consumption based on the user activity trends, in terms of time. Similar to the solar energy, we first quantize the BS workload

energy demand into the workload energy state space, each state enumerated by a non-negative integer. If the workload demanded energy in time slot t is l^*, we quantize the workload energy state as $l_t = \lfloor \frac{l^*}{\Delta_l} \rfloor$. Here, Δ_l is a constant quantization interval. We build a Markov chain for each time slot [31], [14]. We collect the statistics of the quantized data about BS workload energy consumption, and obtain the transition probability between two possible states in every two successive time slots. The BS workload demanded energy transition probability from the ith state to the jth state is $p^l_{i,j}$. Each time slot has its own transition probability matrix $p^{l(t)}_{i,j}$.

The amount of energy taken from the grid in each time slot is g_t, i.e., $g_t = l_t + d_t - s_t$, and the unit is kW. Since the time unit is one hour, kWh is equivalent to kW in this research. The electricity price of the on-grid power associated with each time slot is a_t, and the unit is $\$/kWh$. We regulate each a_t with a reward function $R(a_t)$ in our model. The unit of $R(a_t)$ is $Reward/kWh$. The relationship between a_t and $R(a_t)$ is monotonically decreasing, implying that if price a_t is low, the reward $R(a_t)$ is high. When the electricity price a_t is low, naturally we prefer to drain more electricity from the grid during this time slot to reduce cost. The energy cost for the BS operator is $g_t \times a_t$. The reward in the optimization problem in each time slot is $u_t = g_t R(a_t)$.

2.1.2 Optimal Policy and Objective

In each time slot t, according to the current solar energy state, BS workload demanded energy state and the corresponding transition probabilities for the subsequent time slots, the MDP optimal policy aims to compare each battery action, and then decides how much energy in the battery should be exchanged in the next time slot that will lead to the maximum long term average reward with the largest probability. Let π denote a decision policy, T represent the whole optimization period, and u_t be the reward in each optimization time slot. Denote Π as all the possible policies and

$U(\pi) = \frac{1}{T}\Sigma_{t=1}^{T} u_t$ as the long term average reward, which is a function of policy π. Thus, the objective is to maximize the long term average reward as follows.

$$max_{\pi \in \Pi} U(\pi) \tag{2.2}$$

$$s.t: \quad g_t + s_t - l_t - d_t = 0 \tag{2.3}$$

$$-D_{\max} \leq d_t \leq D_{\max} \tag{2.4}$$

$$0 \leq b_t \leq B \tag{2.5}$$

$$b_{t+1} - b_t = d_t. \tag{2.6}$$

Equation 2.3 imposes the connected components of the energy system to achieve energy equilibrium. Equation 2.4 defines the range that the battery can be charged or discharged in one time unit. Equation 2.5 constrains the battery state to be between zero and its full capacity. Constraint 2.6 means the battery state difference between two successive time slots is the battery action taken in that time slot.

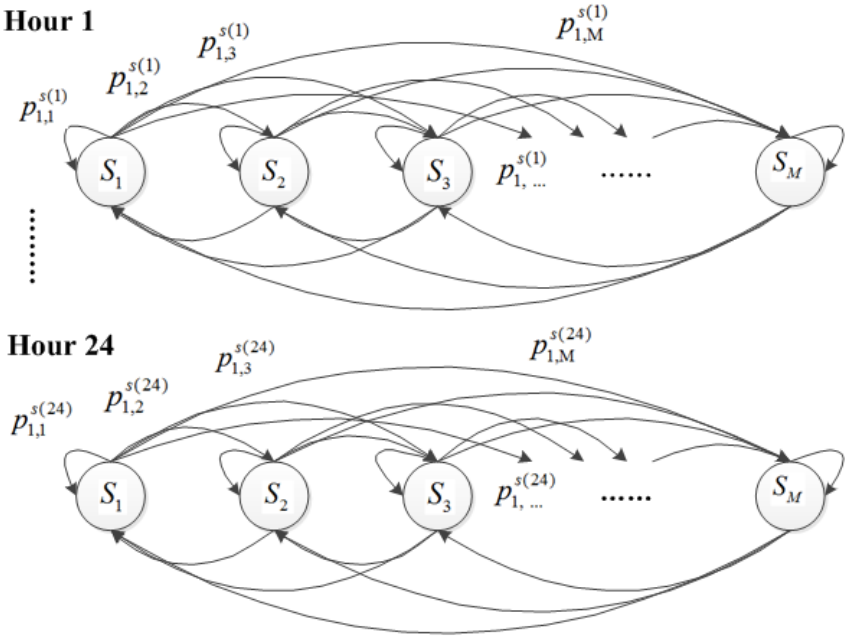

Figure 2.2 State transition diagrams for the solar energy state.

For a particular month or season, we collect the statistics of solar radiation condition for each time slot. For instance, we define the time slot to be an hour in this work. To calculate the transition probability, as mentioned before, according to the historical and quantized data, for each time slot we obtain the transition probability between two possible states in every two successive time slots. For example, consider a typical day in one particular month or season. Collecting the statistics of the quantized records, we find that State 1 at 7 A.M. remains State 1 at 8 A.M. m_1 times, transits to State 2 m_2 times, ..., and transits to State M m_m times, respectively. Then, the corresponding transition probabilities are $p_{1,1}^{s(7)} = \frac{m_1}{m_1 + m_2 + ... + m_m}$, $p_{1,2}^{s(7)} = \frac{m_2}{m_1 + m_2 + ... + m_m}$, ..., $p_{1,M}^{s(7)} = \frac{m_m}{m_1 + m_2 + ... + m_m}$, respectively. All the probabilities $p_{1,1}^{s(7)}, p_{1,2}^{s(7)}, ..., p_{1,M}^{s(7)}$ sum up to 1. The same rule is applied to calculate the transition probabilities of State 2 to other states. This forms one chain and each chain generates a transition probability matrix. We build the Markov chain and transition probability matrix for each time slot (hour), $p_{i,j}^{s(t)}$. This satisfies the nature of solar radiation variations and time variations. For example, we define the available solar radiation strength into 10 levels. Level 1 stands for the weakest radiation level; Level 10 is the strongest level. For instance, at 7 A.M. and 6 P.M, the solar radiation condition may be the same in a day: Level 3. However, at 7 A.M., the solar state has a larger probability to transit to Level 4 in the next hour (8 A.M.) due to sunrise. In contrast, at 6 P.M., the solar state has a larger probability to transit to Level 2 in the next hour (7 P.M.), because of sunset. Therefore, each time slot is characterized by its own transition probability matrix. The Markov solar state transition diagrams are shown in Figure 2.2.

For the BS workload condition, similar to the solar radiation transition probability matrix analysis, we collect the statistics of the BS workload demanded energy value for each time slot (hour), and then build the transition probability matrix for each time slot (hour), $p_{i,j}^{l(t)}$. This satisfies the user (human) activity variations in

terms of time in a certain area. Similar to the analysis of the solar radiation variation, under the coverage of a particular BS, the users have particular trends to transit in or out of this BS at different times. The Markov BS workload demanded energy state transition diagrams are similar to those in Figure 2.2.

Thus, each time slot (hour) has a different transition probability matrix. For example, one day has 24 hours; the solar and BS workload condition transition probability matrices for each hour are $p^{s(1)}, p^{s(2)}, ..., p^{s(24)}$ and $p^{l(1)}, p^{l(2)}, ..., p^{l(24)}$, respectively.

2.1.3 Fast Heuristics

Since the original MDP optimal policy iteration method incurs a high computational complexity, we propose some heuristics to approximate the optimal energy dispatching strategy with low computational complexity. First, the solar radiation level and BS workload energy demand should be represented by a large number of states, but we do not need to search for them all. In our heuristic algorithm, at each decision point, for both the solar state and workload demand state, the algorithm just searches for the top $N(N < n)$ states (i.e., N largest transition probabilities) most likely transitioned from the current state, instead of searching for all the n states in the Markov chain.

We do not search for the states with lower transition probabilities in the algorithm because the probabilities of transitioning from the current state to those states are very small. In other words, those states do not have much contribution on the long term average reward. Eliminating these states does not impact the optimal policy much but can significantly reduce the computational time. The number N depends on the number of states to be quantified. This depends on the accuracy required by the system, and the computational capability of the particular system. If the chosen N is large, the computational time will be prolonged, but the accuracy will be increased, i.e., the solution is more accurate, closer to the optimal one.

Second, we can further reduce the computational complexity by limiting the optimization period Γ. That is, at each decision point, we only determine the optimal battery actions for a few time slots in the near future. For example, one day has 24 hours, and if the optimization period Γ is 12, we should have 2 calculation cycles to complete today's optimization. Having shorter Γ can significantly reduce the computational time at each individual decision point. The optimization period Γ also depends on the number of states to be quantified, the accuracy required by the system, and the particular system's computational capability. If Γ is large, the computation is high but with increased accuracy. If Γ is small, the number of optimization cycles will be increased and the solution accuracy is reduced. High accuracy means the solution obtained is more accurate and closer to the optimal one.

Algorithm 1 Heuristic Algorithm

1: Initial $\forall s_{t+1}, l_{t+1} \in S \times L$ (with N largest transition probabilities states), $\forall d_{t+1}, a_{t+1} \in D \times A, STOP \leftarrow 0$

2: **while** $t = 0, STOP = 0$ **do**

3: **for** each $(s_{t+1}, l_{t+1}) \in S(N) \times L(N), (d_{t+1}, a_{t+1}) \in D \times A$ **do**

4: $U_{t+1} \leftarrow \max_{d_{t+1}}\{r_t + \Sigma_{(s_{t+1},l_{t+1},d_{t+1},a_{t+1})\in S\times L\times D\times A} P_{t+1} \times R_{t+1}\}$

5: **end for**

6: **if** $t = \Gamma$ **then**

7: $STOP \leftarrow 1$

8: **end if**

9: **end while**

10: $\pi(d_{t+1}) \leftarrow \max_{d_{t+1}}\{r_t + \Sigma_{(s_{t+1},l_{t+1},d_{t+1},a_{t+1})\in S\times L\times D\times A} P_{t+1} \times R_{t+1}\}$

In the heuristic algorithm, we first initialize all the states, i.e., available solar energy state, BS workload demanded energy state and battery state, according to

those real conditions in the current time slot. This algorithm will keep searching for all the possible battery actions and compare which action will lead to the largest expected reward. The impact of the selected action (which yields the largest reward) on the subsequent Γ time slots is weighed by the transition probabilities between two successive states. If the optimization period Γ is reached, the algorithm stops. Also, this algorithm can only search for the top N states with the highest transition probabilities from the current state.

2.1.4 Simulation Results

According to the historical solar radiation data and the generated base station workload energy demand data, we quantify both of them into 100 states. In the simulation, we perform the one-day (24 hours) optimization by considering the top 40 and top 25 highest probability states, respectively. In our simulation, the battery may perform five optional actions $d(x) = -2, -1, 0, 1, 2$, and the unit is kWh.

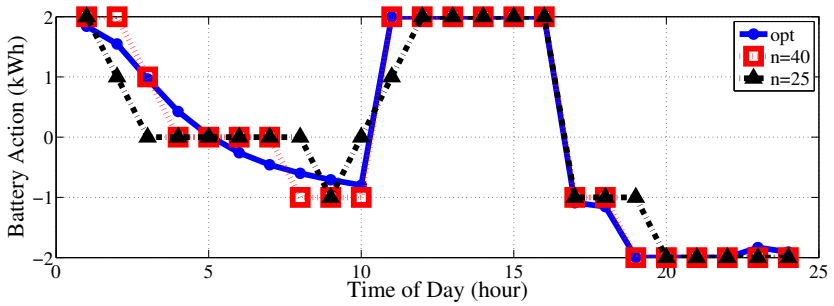

Figure 2.3 Battery action for optimization period t =24 for different n.

Our heuristic algorithm only needs to have the knowledge of the current hour's information, such as the current hour's solar state s_t, BS workload state l_t, and battery condition b_t; it does not need to predict the future hours' solar radiation and BS workload energy demand information. The 24 hours' transition probability matrices for the solar state and BS workload energy demand state ($p_{i,j}^{s(t)} and\ p_{i,j}^{l(t)}$) have been obtained based on the historical data ahead. Electricity prices are known.

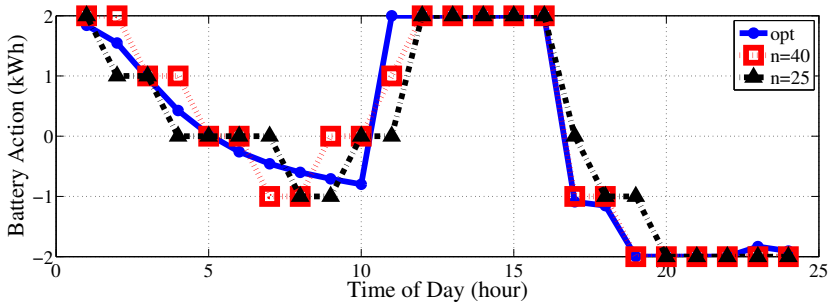

Figure 2.4 Battery action for optimization period t =12 for different n.

Figures 2.2 and 2.3 show the results for t =24 and t =12 hours, respectively. t =12 needs 2 optimization cycles, as compared with t =24. Note that the red curve (n =40) is always closer to the blue curve ("opt") than the black curve (n =25); this is intuitive since the search space corresponding to the red curve with n =40 is larger than that of the black curve with n =25.

In this research, we also observe that the performance of the proposed heuristic algorithm is highly dependent on the fineness of the transition probability matrix, i.e., if the the transition probability matrix is finer, the performance of the heuristic algorithm is better. Therefore, another conclusion is that the accuracy of the "predictor" is the key factor to manage the green energy in the cellular networks.

2.2 Dual-Battery and Min-max RGR User Association Scheme

As mentioned, solar energy generation depends on many factors, such as temperature, sun light intensity, and geolocation. Coverage of a BS also exhibits temporal and spatial diversities, leading to different user densities at different places and times. This mismatch between the green energy generation and workload energy demands in a BS results in inefficient green energy utilization.

In this study (the detail information can be referred to [44]), we invent the dual-battery architecture for green energy harvesting. The dual-battery architecture is shown in Figure 2.5. Unlike most existing works, we do not predict the available

solar energy and solar energy generation rate, or pre-allocate green energy slot by slot. By installing dual-batteries at BSs, the amount of available solar energy for each time period is known and accurate. This time period is called the battery cycle in this work. The operational mechanism is simple, in which the BS consumes the solar energy stored in Battery 1 in the current battery cycle that was harvested in the previous battery cycle. Then, in the next battery cycle, the BS consumes the solar energy stored in Battery 2 that is harvested in the current battery cycle. That is, the two batteries alternate their roles of harvesting and discharging every battery cycle. If the green energy in the battery is sufficient, the BSs directly drain the energy from the batteries in real time. In theory, if the amount of workload demanded energy is more than the available harvested solar energy, the utilization of green energy in our work can reach 100%, thus achieving the goal of furthest saving the on-grid energy consumption.

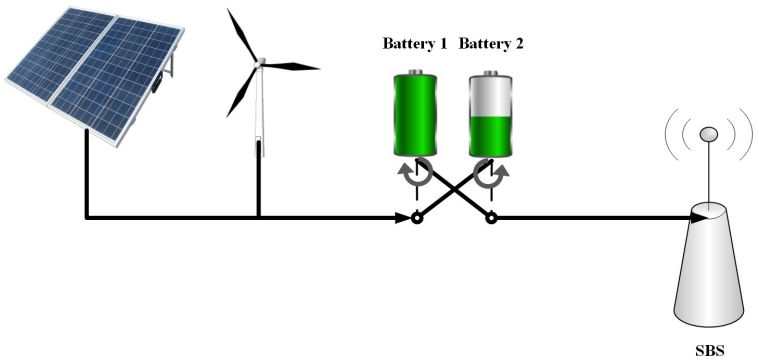

Figure 2.5 Dual-battery architecture.

The advantages of adopting dual-battery at BSs are illustrated as follows. First, by installing dual-battery at each BS, the "prediction" issue is avoided; there is no need to predict the available green energy. The amount of available green energy in the battery is known and accurate. Second, since electric current flow is directional, a single rechargeable battery cannot discharge and be charged simultaneously at a BS. Dual-battery achieves concurrent green energy harvesting and BS powering along

the time domain. There is always one battery harvesting green energy at a BS, and at the same time, one battery is discharging to power the BS; in this sense, the green energy harvesting efficiency is maximized. Third, without energy storage, instantaneously available green energy harvested from the environment at a BS is most likely insufficient to perform effective transmission; by adopting dual-battery, the harvested green energy can be stored and accumulated in each battery for a while to reach a certain energy level, and then be consumed in the next battery cycle.

2.2.1 System Model and Problem Formulation

In this work, we propose a green energy driven user-BS association method to maximize the utilization of green energy at BSs equipped with dual-battery systems. In this network, BSs are powered by both on-grid and solar energy, and have solar panels, wind turbines and dual-batteries installed. In this chapter, we consider a cellular network with multiple macro cell BSs (MBSs) as shown in Figure 2.6. Each MBS is powered by on-grid energy and green energy, and equipped with a dual-battery system. We consider solar and wind energy as the green energy source in this work though other renewal sources can be equally adopted. In our proposed system, the maximum power consumption of a BS is set as P_{total}. If the solar energy stored in the battery is sufficient to power the BS, then the BS directly drains the energy from the battery in real time. If the solar energy in the battery has been exhausted, the BS will draw the on-gird energy.

Consider a cellular network with M mobile users and N BSs. In each battery cycle of T seconds, one battery harvests solar energy through solar panels; at the same time, the other battery discharges its energy to power the BS. The BSs update their cell sizes every τ seconds. T is selected to be an integer multiple of τ. In a battery cycle, the BSs update their cell sizes $\frac{T}{\tau}$ times. BSs update their cell sizes by adapting their pilot signal power and switching on/off their sectors. This enables the

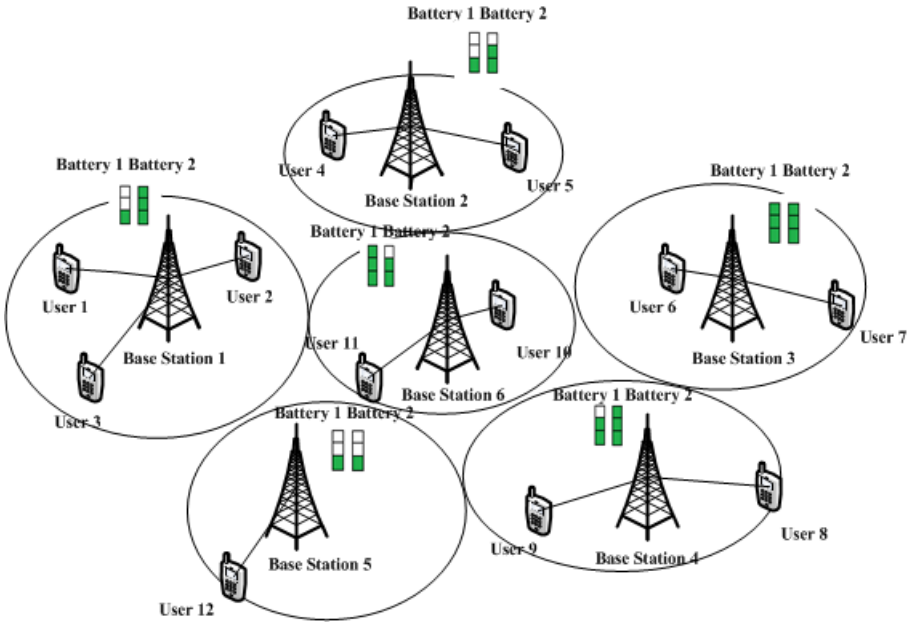

Figure 2.6 Green energy powered cellular network with dual-battery system.

users to be associated with different BSs. The user-BS association matrix at the ith cell size update is $\boldsymbol{X_i} = X_i(k, j)$. Let $X_i(k, j) = 1$ when user k is associated with BS j; otherwise, $X_i(k, j) = 0$, where $k \in \{1, 2..., M\}$ and $j \in \{1, 2..., N\}$. Assume the BSs always have data transmission to mobile users during the τ seconds [22]. The energy consumption of BS j during the ith time slot can be expressed as

$$C_{i,j} = \sum_{k=1}^{M} X_i(k, j) P_{k,j}^{t} \tau + P_j^{static} \tau, \tag{2.7}$$

where $P_{k,j}^{t}$ is the transmission power of BS j for serving user k, $P_{k,j}^{r} = P_{k,j}^{t} \cdot PL_{k,j}$. The received power $P_{k,j}^{r}$ is determined by the user's QoS requirements. $PL_{k,j}$ is the path loss between user k and BS j. P_j^{static} is the static power consumption of BS j.

At the beginning of each battery cycle, the total available solar energy in a battery of BS j is E_j^0, which was harvested in the previous battery cycle. E_j^0 can be different values in the different battery cycles, and has to be less than or equal to the full battery capacity. As time elapses during the battery cycle, the residual solar

energy in the battery of BS j at the ith time slot is $E^r_{i,j}$. $0 \leqslant E^r_{i,j} \leqslant E^0_j$ constrains $E^r_{i,j}$ to be between zero and the initial solar energy E^0_j stored in the battery. $E^r_{i,j}$ at BS j is updated for each time slot i. Since rechargeable energy storage devices cannot both charge and discharge simultaneously [47], that is the reason we propose the dual-battery system. In this dual-battery system, in each battery cycle, one battery is only used to harvest and store solar energy through the solar panel; the other is only used to power the BS. These two batteries supersede their roles in the next battery cycle. In our work, we do not need to predict the solar radiation condition and green energy generation rate. At the beginning of each battery cycle, the available solar energy E^0_j is known and accurate. As time elapses, the residual green energy in the battery $E^r_{i,j}$ will be updated to BSs at each time slot.

We define the residual green energy ratio (RGR) of BS j at the ith time slot of a battery cycle as

$$R_{i,j} = \frac{E^r_{i,j}}{C_{i,j}}. \tag{2.8}$$

Here, as mentioned above, $E^r_{i,j}$ is the residual solar energy stored in the battery of BS j at the ith time slot of the battery cycle; $C_{i,j}$ is the energy consumption for the ith time slot based on the user association at BS j. If $E^r_{i,j} \geqslant C_{i,j}$, then $E^r_{i,j} - C_{i,j} = E^r_{i+1,j}$, which means the solar energy $E^r_{i,j}$ is sufficient to support the energy consumption $C_{i,j}$; subtracting the actual energy consumption from the residual solar energy at the current time slot results in the residual solar energy for the next time slot $E^r_{i+1,j}$. If $E^r_{i,j} < C_{i,j}$, which means the amount of the residual solar energy in the battery cannot afford the energy consumption of the BS in this time slot, then the BS will draw the additional amount of on-gird energy $C_{i,j} - E^r_{i,j}$ to power the BS [27]. Since the user association optimization is achieved within each time slot, for brevity, we just omit the subscript i for the rest of the research. For example, $R_{i,j}$ is simplified as R_j, $C_{i,j}$ is simplified as C_j, and so on.

In order to achieve the optimal green energy driven user association, we aim to minimize the maximal R_j among the N BSs for each time slot. A large R_j is attributed to plentiful available residual solar energy E_j^r and/or small energy consumption C_j at this BS at this time slot. The rationale behind this objective is to allow BSs with larger RGRs to associate with more users. In other words, the BS with more residual solar energy and/or with fewer mobile users at this time slot will try to serve more users by utilizing its green energy, thus increasing the green energy utilization. Therefore, the green energy driven user association optimization problem can be formulated as

$$\min_{X(k,j)} \max\{R_1, R_2..., R_N\} \tag{2.9}$$

$$s.t.: \ C_j \leqslant P_{total}\tau \tag{2.10}$$

$$\sum_j X(k,j) = 1 \tag{2.11}$$

$$\sum_k \sum_j X(k,j) = M. \tag{2.12}$$

Since the transmission power of a BS is bounded and the BS cannot absorb unlimited mobile users, Equation 2.10 imposes the BS energy consumption C_j to be less than or equal to the maximum power consumption of a BS in each time slot. Equation 2.11 guarantees that a user is associated to only one BS and Equation 2.12 guarantees that all users in this network are served.

Theorem 1. *The problem that minimizes the maximal residual green energy ratio is NP-hard.*

Proof. Consider a case of the problem with only two BSs. By assuming the BSs have the same amount of solar energy, the communications energy consumption of each BS determines R_j. Each user k can be covered by either BS 1 or BS 2 in this time slot. $\boldsymbol{K_1}$ and $\boldsymbol{K_2}$ denote the two user sets representing the users associated with BS

1 and BS 2, respectively, i.e.,

$$\begin{cases} X(k,1) = 1, k \in \boldsymbol{K_1}; \\ X(k,2) = 1, k \in \boldsymbol{K_2}. \end{cases} \tag{2.13}$$

$\boldsymbol{K_1} \cup \boldsymbol{K_2} = \boldsymbol{K}$, and $\boldsymbol{K}$ is the set, which includes all the users in this network. If a set of users associate with BS 1, the residual green energy ratio is R_1; if a set of users attach to BS 2, the ratio is R_2. Minimizing the maximal residual green energy ratio equals to finding the subset $\boldsymbol{K_1} \subseteq \boldsymbol{K}$ that satisfies

$$R_1 = R_2. \tag{2.14}$$

By restricting the simple case of the problem to $R_1 = R_2$, and assuming the total amount of energy consumption be evenly divisible by 2, the problem equals to the partition problem [16], which is a well-known NP-hard problem. □

2.2.2 Heuristic Algorithm

Since minimizing the maximal residual green energy ratio is NP-hard, the optimal solution cannot be obtained in polynomial time. Therefore, we introduce heuristics to solve this problem and at the same time avoid the ping-pong process, i.e., a nominal greedy algorithm that dissociates users from a BS with smaller RGR and associates them with the BS with the largest RGR will likely enrich the original BS to become the one with the largest RGR, and will thus attract the users back to the original BS, and vice versa. Therefore, to solve this problem, we first introduce the concept of the energy dependent set (EDS).

Definition 1. *Let R_j be the RGR of BS j at the current time slot. Then, EDS $\boldsymbol{D} = \{j | R_j = \delta, j \in \{1, 2..., N\}\}$, where δ is the largest RGR among the N RGRs prior to the user association optimization at this time slot.*

Guideline 1. *Every BS in EDS with the largest RGR should absorb users from BSs outside EDS by increasing its pilot signal power level and switching its sectors on. The users once absorbed in a BS within EDS cannot be associated with those outside EDS within the same time slot. When the BS in EDS enlarges its cell size and switches on its sectors, the neighboring BSs outside EDS should shrink their cell sizes or switch off their sectors accordingly.*

Algorithm 2 Heuristic Algorithm

1: Initial user-BS association and E_j^0, $j \in \{1, 2..., N\}$;
2: In each time slot, calculate and sort R_j from the largest to the smallest, and find δ and δ';
3: Find the set $\boldsymbol{D}$ such that $R_j = \delta, \forall j \in \boldsymbol{D}$
4: **for** $n = 1$ to $|\boldsymbol{D}|$ **do**
5: Associate more users to the BSs in EDS, and R_j will be decreased;
6: **if** $R_j \geqslant \delta'$ **then**
7: Continue to assign more users to the BSs in EDS;
8: **end if**
9: **end for**
10: Return the user-BS association;

Guideline 1 engineers the design of this heuristic algorithm from two aspects: 1) to feasibly solve the problem of minimizing the maximal residual green energy ratio with low computational complexity, and 2) to identify which BSs in EDS should increase their pilot power and adapt their sectors, and which BSs outside EDS should reduce their pilot power or switch off sectors within the same time slot. The pseudo code of this heuristic algorithm is shown in Algorithm 2.

2.2.3 Simulation Results

In our work, we aim to maximize the green energy utilization of the whole cellular network. Therefore, we consider the total harvested solar energy utilization in this network and compare the utilizations between our algorithm and the Strongest Signal First (SSF) algorithm [71] under the same simulation setting, i.e., the same number of users and the same total solar energy of 120 kWh harvested by these 6 BSs in one battery cycle. At the end of each battery cycle, the more solar energy leftover in the batteries implies that more on-grid energy has to be drawn. We consider three scenarios: 1) network with high user density with 210 users, 2) network with low user density with 90 users, and 3) network with medium user density with 150 users. Figure 2.7 shows the performance of the two algorithms for Scenario 1. At the first several time slots, these two algorithms achieve almost the same performance since all the BSs have the solar energy to consume. As time elapses, in the middle part of the battery cycle, since SSF can neither change BS cell size nor modify the user associations, some of the BSs with more users exhaust the solar energy in their batteries earlier while others with fewer users still have residual solar energy left in their batteries. On the contrary, our algorithm can change the cell size and adapt user associations among BSs; the BS with a larger RGR will serve more users as compared with the BS with a smaller RGR. Thus, as shown in Figure 2.7, our proposed algorithm consistently draws down the solar energy in the batteries. This highly dense network incurs large energy consumption. At the end of battery cycle, for both algorithms, their solar energy is used up and on-grid energy is drawn to power their BSs.

Scenario 2 with low user density also implies less energy consumption in the network. As shown in Figure 2.8, these two algorithms exhibit almost the same performance because all BSs have relatively plentiful solar energy to utilize. They can all draw the solar energy to power the BSs. Since the total available solar energy is more than the total BS workload demanded energy, in the end of the battery cycle,

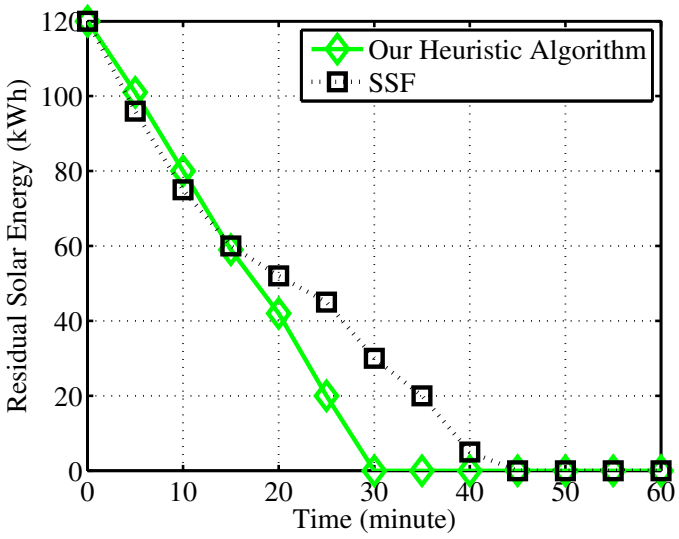

Figure 2.7 First scenario, network with high user density.

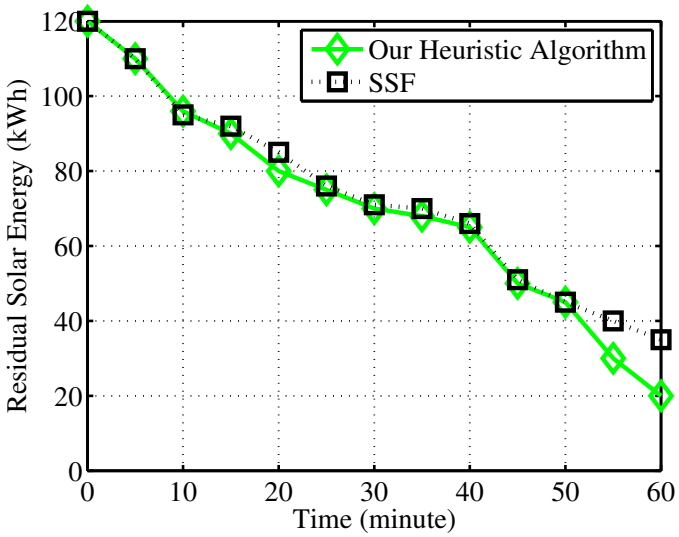

Figure 2.8 Second scenario, network with low user density.

there are still some residual solar energy left in the batteries. In this scenario, both of the algorithms will not consume on-grid energy.

In theory, if the amount of workload demanded energy is more than the available harvested solar energy, the utilization of green energy in our work can reach 100%, thus achieving the goal of furthest saving the on-grid energy consumption. However, in each time slot optimization, the BS with maximal RGR may be assigned an

excessive number of mobile users. Thus, traffic delivery latency is a potential issue of this green energy driven user association scheme.

2.3 Dual-Battery Enabled Profit Driven User Association Scheme

Most existing works propose user-BS association schemes aiming to associate more mobile users to the BSs, which have relatively abundant green energy, to maximize the green energy utilization. This is seemingly rational, but brings latent negative effects. First, disassociating users from the original BS and associating them to other far away BSs will incur higher transmission power to serve these users, because of the channel attenuation. This will exhaust the green energy quicker at those BSs or even consume more on-grid energy if those BSs do not have enough residual green energy to accommodate a larger number of users at once [13]. Second, a large number of users crowded at a BS will lead to heavy traffic congestion and high traffic delivery latency [28]. More mobile applications nowadays impose stringent requirements on the traffic delivery latency [17].

Here, we first review some related works on user association for traffic load balancing and user association for green energy utilization maximization in cellular networks.

User association on traffic load balancing: Balancing traffic load in cellular networks has been extensively studied in recent years [6]. The most practical traffic load balancing approach is the cell range expansion technique that biases user's receiving signal-to-interference-and-noise-ratios (SINRs) from some BSs to prioritize these BSs in associating with users [15]. A large bias is usually given to small BSs to offload users, owing to the different transmission power of macro BSs and small BSs [6]. Deriving the optimal bias for BSs is challenging. Singh *et al.* [58] investigated the impact of the bias on network performances and provided a comprehensive analysis on traffic load balancing using cell range expansion. An α-optimal user

association algorithm was proposed by Kim *et al.* [31] to achieve flow level load balancing under spatially heterogeneous traffic distribution. The result of convex optimization varies by selecting the different values of α. Ye *et al.* [66] modeled the traffic load balancing problem as a utility maximization problem and developed distributed user association algorithms using the primal-dual decomposition. Aryafar *et al.* [9] applied game theory to solve the traffic load balancing problem. They modeled the problem as a congestion game in which users are the players and user association decision are the actions. Tam *et al.* [59] proposed a new strategy on load balancing in the downlink of a heterogeneous network by considering the backhaul capacity at each BS to maximize the network sum rate.

User association on green energy utilization maximization: In cellular networks, green energy utilization can be improved by associating mobile users among different BSs, according to the available green energy at individual BSs. Zhou *et al.* [70] proposed a handover parameter tuning algorithm for target cell selection, and a power control scheme for coverage optimization to guide mobile users to access the BSs with green energy supply. Liu and Ansari [44] proposed a user association scheme to maximize the utilization of green energy by associating more users to the BSs with relatively abundant green energy. Huang *et al.* [28] proposed a user association algorithm to maximize the green energy utilization but the convergence of the heuristic algorithm may not be guaranteed in some cases. A user association framework was proposed to enhance the green energy utilization in cellular networks, but most existing green energy related works simply assume that the amount of green energy can be predicted and pre-allocated to the BSs along the time domain [24]. Actually, it is hard to engineer their algorithms in practice. Liu and Ansari [40] jointly considered the green energy utilization and traffic delivery latency, but their proposed heuristic algorithm does not have a traffic latency feedback mechanism,

implying that new traffic congestion may be induced in maximizing the green energy utilization.

Taking into account of these issues comprehensively, in this research, we propose the dual-battery enabled profit driven user association scheme in a heterogeneous cellular network by jointly considering the green energy utilization and traffic delivery latency. Since this profit driven user association optimization problem is NP-hard, we further provide some heuristics to maximize the total profit with low computational complexity.

Degraded services lead to dissatisfaction on user experience that may eventually lose customers and profits. According to current mobile service pricing policy, network providers charge all the users subscribing the same level of service plan with the same rate. However, users subscribing the same service plan may experience different services in realty. Hence, in this work, we propose a novel pricing model based on the real time service quality. Each user prepays to subscribe a level of service plan. Each level of service plan has a guaranteed service quality threshold. If the user's received service is better than this quality threshold, the network providers can earn 100% of the user's prepayment. If the user's received service is worse than this quality threshold, the network provider can only charge a percentage of the prepayment. The worse service received by the user, the less percentage of the prepayment the network provider can charge. This pricing model incentivizes the network providers to provide better service quality to earn their profit as well as benefits mobile users.

In this research (the detail information can be referred to [41]), we consider one macro cell in a heterogeneous cellular network. In each macro cell, there is one macro BS (MBS) and multiple small BSs (SBSs), as shown in Figure 2.9. MBS has higher transmission power than that of SBS. MBS and SBSs are equipped with solar panel, wind turbine and dual-battery, and can be powered by both on-grid brown energy and green energy. We consider solar energy and wind energy as the green energy source

in this work though other green sources can be equally adopted. In the following analysis, a BS generally refers to an MBS or an SBS. Denote $\mathcal{B}$ as the set of BSs in a macro cell including both MBS and SBSs. The number of BSs in a macro cell is J; the BSs are indexed by j.

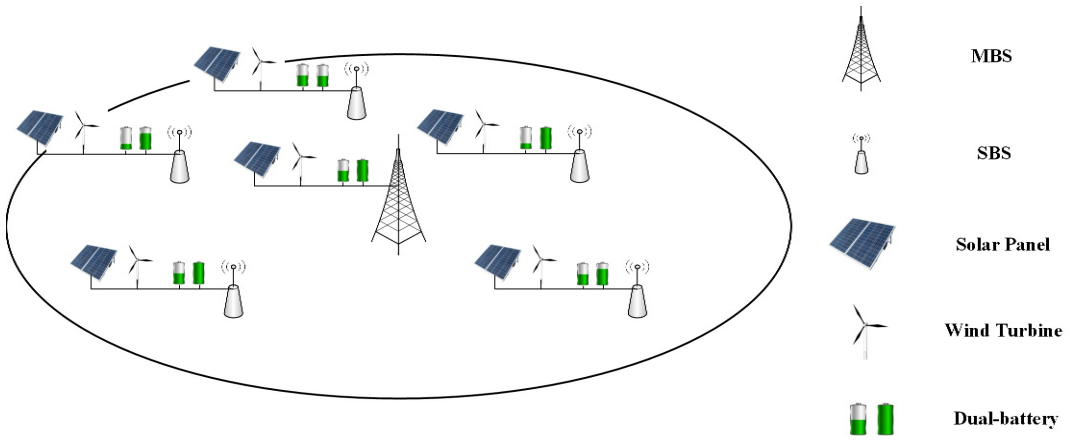

Figure 2.9 Framework of a green heterogeneous cellular network.

In a cellular network, the time scale of per-user channel and traffic variations is up to tens of seconds; the time scale of the aggregated traffic demand variations in a BS is tens of minutes [11]. The user association parameters are usually adapted based on the aggregated traffic demand of a BS rather than that of an individual user [11], [25]. Because of the difference in the time scales of per-user traffic variations and that of the user association parameter, the impact of the user association algorithms on a BS's performance can be evaluated by using the steady-state model, e.g., queuing models, without considering individual users' instantaneous channel and traffic variations [31]. Therefore, we can model the downlink traffic and traffic delivery latency based on queuing and the time scale of a time slot for user association is tens of minutes. The time duration and index of a time slot are τ and t, respectively. The system models, problem formulation, heuristic algorithm and simulation results are presented as follows.

2.3.1 Dual-battery Model

We denote Γ as the length of the battery cycle and Γ is selected to be an integer multiple of user association parameter adaption time slot τ. Both Γ and τ are quantified in minutes. At the beginning of each battery cycle, the initial total harvested green energy in a battery of BS j is E_j^0, which was harvested in the previous battery cycle. E_j^0 can be different in different battery cycles at the same or a different BS j, and has to be less than or equal to the full battery capacity. As time elapses during the battery cycle, the residual green energy in the battery of BS j at the tth time slot is $E_j(t)$. $E_j(t)$ is to be between zero and the initial green energy E_j^0 stored in the battery, i.e., $0 \leqslant E_j(t) \leqslant E_j^0$. $E_j(t)$ at the BS j is updated for each time slot t.

2.3.2 Traffic Model

We consider the BSs are deployed to provide downlink data transmission in a macro cell. Since provisioning the profit driven green cellular networks is a network planning problem, the user association solution depends on the traffic generation of a target area. Therefore, in this research, we adopt a location-based traffic model. In the tth time slot, the traffic (data requests) is assumed to arrive at location x according to a Poisson process with the average arrival rate which equals to $\lambda(x,t)$ per second, and the traffic size (packet size) per arrival satisfies a general distribution with the average traffic size of $\nu(x,t)$ bits. Here, $\lambda(x,t)$ and $\nu(x,t)$ can be derived based on the statistics of traffic data from traffic measurements; they may have different values in different time slot t.

We assume that there is only one user at location x. When a mobile user at location x is associated with the jth BS, the user's data rate $r_j(x)$ can be generally expressed as a logarithmic function of the perceived signal-to-interference-plus-noise ratio (SINR), i.e., $SINR_j(x)$, according to the Shannon-Hartley Theorem [56],

$$r_j(x) = W_j(1 + SINR_j(x)). \tag{2.15}$$

Here, W_j is the bandwidth in BS j, and

$$SINR_j(x) = \frac{p_j g_j(x)}{\sigma^2 + \sum_{m \in \boldsymbol{\mathcal{I}_j}} I_m(x)}. \tag{2.16}$$

Note that p_j is the transmission power of BS j; $g_j(x)$ is the channel gain between BS j and the user at location x; σ^2 denotes the noise power level. $\boldsymbol{\mathcal{I}_j}$ represents the set of interfering BSs and is defined as the set of BSs which interfere the jth BS's transmission. $I_m(x)$ is the average interference seen by a user at location x from the mth BS.

In cellular networks, various downlink scheduling algorithms have been proposed to properly share the limited radio resource in a BS. For analytical simplicity, we assume that mobile users at a BS are served based on the round robin fashion. Then, the average traffic load density at location x in BS j is calculated as

$$\varrho_j(x,t) = \frac{\lambda(x,t)\nu(x,t)\eta_j(x)}{r_j(x)}. \tag{2.17}$$

Here, $\frac{r_j(x)}{\nu(x,t)}$ is the service rate provisioned by BS j. $\eta_j(x)$ is an indicator function. If $\eta_j(x) = 1$, the use at location x is served by BS j; otherwise, the user is not served by the BS. $\boldsymbol{\eta} = (\eta_1(x), ..., \eta_J(x))$. Denoting $\boldsymbol{\mathcal{A}}$ as the coverage area of the macro cell, the traffic load on the jth BS can be expressed as

$$\rho_j(t) = \int_{x \in \boldsymbol{\mathcal{A}}} \varrho_j(x,t) dx. \tag{2.18}$$

This value of $\rho_j(t)$ indicates the utilization of BS j, i.e., the fraction of time BS j is busy in the tth time slot.

Since the traffic arrival (user requested data) processes for individual users are independent and Poisson, the traffic arrival at the j BS is the sum of the traffic arrivals of users associated with it, i.e., $\int_{x \in \boldsymbol{\mathcal{A}}} \lambda(x,t)\eta_j(x)dx$, which still follows a Poisson process. The BS's service rate $\frac{r_j(x)}{\nu(x,t)}$ follows a general distribution. Assuming mobile

users share the BS's radio resources and are served based on the round robin fashion, consequently, the downlink traffic delivery in the BS realizes an M/G/1-PS (processor sharing) queue [32].

A mobile user at location x, who is associated with BS j, is assumed to have average traffic size $\nu(x,t)$ in the tth time slot. To fulfill the user's traffic demand, the required service time is

$$\gamma_j(x,t) = \frac{\nu(x,t)}{r_j(x)}. \tag{2.19}$$

According to [32], since the traffic delivery process in a BS realizes a M/G/1-PS queue, the average traffic delivery time for the user in BS j is

$$T_j(x,t) = \frac{\nu(x,t)}{r_j(x)(1-\rho_j(t))}. \tag{2.20}$$

The average waiting time for the traffic load $\nu(x,t)$ in BS j is

$$W_j(x,t) = T_j(x,t) - \gamma_j(x,t) = \frac{\rho_j(t)\nu(x,t)}{r_j(x,t)(1-\rho_j(t))}. \tag{2.21}$$

Denote $\mu_j(x,t)$ as the latency ratio of BS j for a user at location x in time slot t, and it indicates how much time a user must "sacrifice" at BS j in waiting for per unit service time,

$$\mu_j(x,t) = \frac{W_j(x,t)}{\gamma_j(x,t)} = \frac{\rho_j(t)}{(1-\rho_j(t))}. \tag{2.22}$$

Since $\mu_j(x,t)$ only depends on the traffic load in BS j and time slot t, we define

$$\mu_j(\rho_j(t)) = \frac{\rho_j(t)}{(1-\rho_j(t))} \tag{2.23}$$

as the latency ratio of BS j. For simplicity, we use $\mu_j(t)$ to represent $\mu_j(\rho_j(t))$. $\mu_j(t)$ is a strictly increasing function of $\rho_j(t)$. A larger $\mu_j(t)$ indicates that BS j introduces higher latency to its associated users.

Proposition 2. *$\mu_j(t)$ is a strictly increasing function.*

Proof. Since

$$\mu_j(t) = \frac{\rho_j(t)}{(1-\rho_j(t))}, \tag{2.24}$$

the first order derivative of $\mu_j(t)$ is

$$\mu_j'(t) = \frac{(1-\rho(t)) - \rho(t)(-1)}{(1-\rho(t))^2} = \frac{1}{(1-\rho(t))^2}. \tag{2.25}$$

Since $\mu_j'(t) > 0$, $\mu_j(t)$ is a strictly increasing function.

□

2.3.3 Pricing Model

In order to incentivize the network provider to provision better service quality, i.e., shortening the traffic delivery latency, and to enhance the fairness among the mobile users, a novel pricing model is introduced. In this pricing model, each user prepays, for example, to subscribe a level of service plan for one month. The payment includes two parts. The first part is network admission fee. The admission fee payment of a user per month can be pro-rated (converted) to every time slot as c_d (in \$), which is charged for every time slot. The second part is service fee. The pro-rated (converted) service fee is c_u (in \$), which is only charged when the mobile user is served in that time slot. c_u is much larger than c_d. Assume this price is determined by market research, and agreeable to both the mobile users (customers) and network provider.

Since the proposed BS transmission system is time slotted, when a mobile user is served by BS j in a time slot, the network provider charges

$$c_r = c_d + c_u\theta_j. \tag{2.26}$$

Here, θ_j is a function reflecting/mapping the latency ratio of BS j to the revenue,

$$\theta_j = \begin{cases} 1, & \mu_j(t) \le \mu_{thres} \\ \frac{1}{\mu_j(t)}, & \mu_j(t) > \mu_{thres} \end{cases}, \tag{2.27}$$

where μ_{thres} is the service plan guaranteed latency ratio threshold and $\mu_{thres} > 1$. If the user experienced latency in that time slot is less than or equal to the network provider's promised traffic latency threshold μ_{thres}, i.e., the service, in terms of traffic delivery latency, is good enough, the network provider can earn 100% of the user's prepayment; otherwise, it can only earn a percentage of the user's prepaid payment. According to Equation 2.27, the higher traffic latency is experienced by the user, the network provider earns a less percentage, θ_j, of the user's prepayment and has to refund $c_u(1-\theta_j)$ to the user. Suppose the number of mobile users who are scheduled to be served by BS j in time slot t is L_j; the revenue gained at the jth BS in time slot t is

$$R_j = L_j c_r. \tag{2.28}$$

2.3.4 Energy Model

The BS's energy consumption includes two parts: the static energy consumption and the dynamic energy consumption [10]. The static energy consumption is the energy consumed by a BS without carrying any traffic load. The dynamic energy consumption refers to the additional energy consumption incurred by traffic load in the BS, which can be represented by a linear function of the traffic load in a time slot [10]. As the BS performs the full transmission power, $\rho_j(t)$ indicates the fraction of time BS j is busy in the tth time slot [30]. The time slot duration is τ. Denote p_j^s as BS j's static power consumption in a time slot. Then, BS j's energy consumption in the tth time slot is

$$P_j(t) = p_j \rho_j(t)\tau + p_j^s \tau. \tag{2.29}$$

Here, $\rho_j(t)\tau$ is the amount of time within a time slot that BS j performs downlink transmission to serve users.

According to the residual green energy $E_j(t)$ and energy consumption $P_j(t)$, the on-grid energy consumed in the jth BS in time slot t is

$$G_j = \{P_j(t) - E_j(t)\}^+, \tag{2.30}$$

where the positive function $\{\bullet\}^+ = max\{\bullet, 0\}$. We denote the on-grid electricity price as c_e (in \$/kWh).

2.3.5 Problem Formulation

In this work, we aim to maximize the profit for the network provider by considering the BS's traffic delivery latency and green energy utilization. We have obtained the traffic latency ratio reflected revenue and the cost of on-grid energy in the macro for each time slot. The dual-battery enabled profit driven user association optimization problem can be formulated as

$$\max_{\boldsymbol{\eta}} (\sum_{j \in \boldsymbol{\mathcal{B}}} R_j - c_e \sum_{j \in \boldsymbol{\mathcal{B}}} G_j) \tag{2.31}$$

$$s.t.\ 0 \leq \rho_j(t) < 1, \tag{2.32}$$

$$\sum_{j \in \boldsymbol{\mathcal{B}}} \eta_j(x) = 1. \tag{2.33}$$

In Equation 2.31, the first item is the traffic latency reflected revenue and the second item is the cost of on-grid brown energy. Equation 2.32 is to guarantee the queuing system in each BS J is stable. Equation 2.33 implies each active user is associated with a BS. This dual-battery enabled profit driven user association optimization problem is NP hard.

Proposition 3. *The dual-battery enabled profit driven user association optimization problem is NP-hard.*

Proof. This profit maximization user association optimization problem is equivalent to (can be converted to) the cost minimization user association problem because

provisioning service to mobile users incurs cost, such as energy consumption and traffic latency increment, from the perspective of network provider. Since the weighted vertex cover problem is a well-known NP hard problem [16], we will reduce it to the cost minimization user association problem.

For a given instance of weighted vertex cover problem with a graph $\boldsymbol{D} = (\boldsymbol{V}, \boldsymbol{E})$, $v \in \boldsymbol{V}, e \in \boldsymbol{E}$. Here, v stands for the vertex and e represents the edge. Each vertex has its weight $a_v \geq 0$. In this problem, the goal is to find a subset of vertexes $\boldsymbol{V'} \subseteq \boldsymbol{V}$ that covers all the edges $e \in \boldsymbol{E}$ in this graph with the minimum total weight, i.e., $\min \sum_{v \in \boldsymbol{V'}} a_v x_v$. Here, $x_v \in \{0, 1\}$ indicates that vertex v is either in subset $\boldsymbol{V'}$ or not.

We construct an instance of cost minimization user association problem. Suppose the user $e \in \boldsymbol{E}$ can be associated to surrounding BS $v \in \boldsymbol{V}$ within the macro cell. Here, e stands for the user and v represents the BS. In each time slot, all the active users e should be served by their surrounding BSs. Serving a user by different BSs incurs different costs $a_v \geq 0$ (equivalent to the "weights" in the weighted vertex cover problem), in terms of traffic latency or the on-grid energy expenses. The goal is to find the subset of BSs $\boldsymbol{V'} \subseteq \boldsymbol{V}$ serving all the active users $e \in \boldsymbol{E}$ with proper user-BS association $x_v \in \{0, 1\}$ that leads to the minimum cost, i.e., $\min \sum_{v \in \boldsymbol{V'}} a_v x_v$.

Since the weighted vertex cover problem can be reduced to the cost minimization user association problem, and the cost minimization user association problem is equivalent to the profit maximization user association problem. Therefore, the profit driven user association optimization problem is NP-hard. □

2.3.6 The Heuristic Algorithm

Since the profit driven user association optimization problem is NP-hard, the optimal solution cannot be obtained within polynomial time. Therefore, we provision some heuristics to maximize the profit with low computational complexity. Modifying

user-BS association in a cellular network, on one aspect, can adjust the traffic latency among the BSs, and on the other one aspect, can change the BSs' transmission energy consumption to enhance the green energy utilization in the network. In order to maximize the profit for the network provider, according to the objective function, the intuition can be seen from two perspectives. The first is to associate users from the BSs with high traffic delivery latency to the less congested BSs to gain the revenue. The second is to let the BSs having more green energy to absorb more users to reduce the cost of on-grid electricity. Therefore, based on the system model, in the PDU heuristic algorithm, the BSs with relatively abundant residual green energy $E_j(t)$ and small traffic delivery latency ratio $\mu_j(t)$ are the candidate BSs to serve more surrounding users.

We first define the residual green energy to traffic latency ratio, $H_j = \dfrac{E_j(t) + \varepsilon}{\mu_j(t)}$. Here, ε is an arbitrary small positive constant to guarantee H_j to be positive, even if the amount of residual green energy $E_j(t)$ at a BS is zero. Also, in order to avoid the ping-pong process (i.e., a nominal greedy algorithm that may dissociate users from a BS first and then attract the users back later to the original BS) [40], we stipulate that the mobile users once associate to other BSs will not be associated back to the original BS within the same time slot.

In the heuristic algorithm, the user-BS association is initialized based on the default user-BS association scheme, strongest-signal-first (SSF) scheme [24], i.e., the users are initially associated to the BS with the strongest signal. For each time slot, sort H_j from the largest to the smallest, and index the BSs by k, ranging from 1 to J. Find the BS with the largest H_k, and define the set $\boldsymbol{\mathcal{B}}_{\boldsymbol{k}}^{\boldsymbol{'}}$, which includes all the adjacent BSs around BS k, $|\boldsymbol{\mathcal{B}}_{\boldsymbol{k}}^{\boldsymbol{'}}| = B_k'$. Then, sort the H_j for the BSs in set $\boldsymbol{\mathcal{B}}_{\boldsymbol{k}}^{\boldsymbol{'}}$ from the smallest to the largest, and index the BSs in this set by y, ranging from 1 to B_k'. Sort the SINRs between the users originally associated with BS k and the yth BS, from the highest to the lowest, and index the users with respective SINRs by l,

ranging from 1 to L. Suppose the number of users at BS y is L_y. Define the initial total profit of all the BSs in the macro cell as M', and after each iteration, denote the total profit as M. The pseudo code of this heuristic algorithm is shown in Algorithm 3.

In this heuristic algorithm, by sorting H_j from the highest to the lowest, the BS with the highest H_j is to serve more surrounding users because it has more abundant green energy and/or lower traffic delivery latency. Its adjacent BS in $\boldsymbol{\mathcal{B}_k^{'}}$ which has the lowest H_j is the one to be offloaded immediately because this BS has less residual green energy and/or higher traffic latency ratio. According to the sorted SINRs between the users and the BS with the highest H_j, users are associated to the BS k one by one. This guarantees that the increment of the energy consumption and that of latency ratio at BS k increase gradually. Calculating the total profit after each iteration, we set three joint conditions to continue the next iteration, 1) the total amount of profit is greater than that of previous iteration; 2) we add a latency feedback mechanism, i.e., BS k should satisfy $\mu_k(t) < \mu_{thres}$; 3) the BS with the higher H_j still has enough green energy to serve more surrounding users. Otherwise, the PDU heuristic algorithm stops the current loop, maintains the previous iteration's user association and starts the next loop. Since our heuristic algorithm uses sorting and avoids the ping-pong process to guarantee convergence, it can avoid unnecessary search to reduce the runtime.

The PDU heuristic algorithm has three sorting procedures and three loops. The computational complexity of sorting J BSs is $O(J \log J)$. The computational complexity of sorting B'_k BSs around BS k is $O(B'_k \log B'_k)$. The computational complexity of sorting L_y user at BS y is $O(L_y \log L_y)$. Assuming the heuristic algorithm search all the BSs and users in the macro cell, the worst case computational complexity of PDU heuristic algorithm is $O(J^3 Z^2 \log(J + Z))$, with respect to the

Algorithm 3 The PDU Heuristic Algorithm

Initialize the user-BS association based on SSF, calculate M' and calculate H_j for all BSs, $j \in \{1, 2, ..., J\}$;
Sort the BSs from the highest H_j to the lowest H_j, and index the BSs by k, $k \in \{1, 2, ..., J\}$, find the BS with the largest H_k;
for $k = 1$ to J **do**
    Denote the set of BSs around BS k as $\boldsymbol{\mathcal{B}}_{\boldsymbol{k}}^{'}$, $|\boldsymbol{\mathcal{B}}_{\boldsymbol{k}}^{'}| = B_k'$, index the BSs in $\boldsymbol{\mathcal{B}}_{\boldsymbol{k}}^{'}$ by y , and sort the BSs from the smallest H_y to the largest H_y;
    for $y = 1$ to B_k' **do**
        Sort the SINRs between the users originally associated with BS k and the yth BS, from the highest to the lowest, and index the users with respective SINRs by l; the number of scheduled users is L_y;
        for $l = 1$ to L_y **do**
            Associate user l to BS k and calculate the current profit as M;
            if $M < M' \parallel \mu_k(t) > \mu_{thres} \parallel E_k(t) < P_k(t)$ **then**
                Maintain the user association of the previous iteration and stop the current loop;
            else
                $M \rightarrow M'$, continue to do the next iteration, i.e., associate the next user;
            end if
        end for
    end for
end for
Return the user-BS association $\boldsymbol{\eta}$;

number of BSs J and number of users Z. Theoretically, this PDU heuristic algorithm is a pseudo polynomial time algorithm.

2.3.7 Simulation Results

Simulations are set up to evaluate the performance of the proposed heuristic solution for maximizing the profit of the network provider in a macro cell. In the simulation, we consider six BSs deployed in a $5km \times 5km$ area; one MBS is located at the center of macro cell and five SBSs are deployed surrounding the MBS. Their locations are fixed, as shown in Figure 2.9. The mobile users are distributed to represent the traffic generation in that area according to the historical traffic statistics which are randomly generated in the simulations. The channel propagation model is based on COST 231 Walfisch-Ikegami distance-dependent channel model [2]. The channel model and parameters are summarized in Table 2.1. Here, PL_{MBS} and PL_{SBS} are the path loss between the users and MBS and SBS, respectively. d is the distance between users and BSs. The total bandwidth is 10 MHz, and the spectrum reuse factor is 1.

The time slot τ is 20 minutes and the battery cycle is 60 minutes. In simulations, each user pays \$100 per month to the network provider, i.e., \$20 is the network admission fee and \$80 is the service fee. The pro-rated prepaid admission fee and service fee for each time slot are $\$9.25 \times 10^{-3}$ and $\$3.7 \times 10^{-2}$, respectively. The on-grid electricity price for powering BS is 6.92×10^{-2}\$/kWh. The initial available green energy E_j^0 at the beginning of the battery cycle for the six BSs are randomly assigned between 0.8kWh and 1.6kWh, and we set the amount of total initial available green energy at these six BSs to be 8kWh.

In the simulations, our proposed PDU heuristic algorithm first initiates the user association based on the SSF scheme, which associates users to the BS with the strongest received signal. The network set-up topology and initial user-BS association

Table 2.1 Channel Parameters

Parameters	Values
$PL_{SBS}(dB)$	$PL_{SBS} = 140.7 + 36.7log_{10}(d[km])$
$PL_{MBS}(dB)$	$PL_{MBS} = 113.1 + 37.6log_{10}(d[km])$
Shadowing	$10dB$ Log Normal Fading
Antenna gain	$15dB$
Noise power level	$-174dBm$

is shown in Figure 2.10. The six red circles are the six BSs. The other six kinds of colored circles denote the six groups of users associated with the six BSs, respectively.

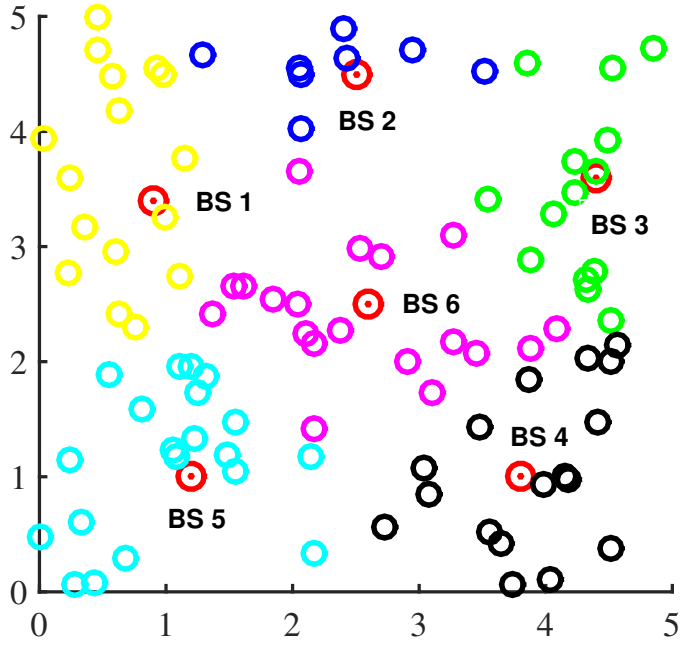

Figure 2.10 Network set-up topology and initial user association.

According to the proposed PDU heuristic algorithm, the BSs with larger H_j will serve more mobile users from their surrounding BSs with smaller H_j. In Figure 2.11, BS 6 is the BS with the largest H_j in this experiment. It first intends to absorb more users from its surrounding BS with the smallest H_j, i.e., BS 5 in this experiment.

In each iteration, it serves one more user from BS 5. When BS 6's residual green energy is insufficient to serve more users, or the latency ratio of BS 6 reaches the predefined threshold, or serving one more user from BS 5 leads to more cost, BS 6 stops absorbing more users. Figure 2.11 shows that BS 6 associates some users from BS 5. The purple stars stand for the users associated with BS 6 after modifying user association.

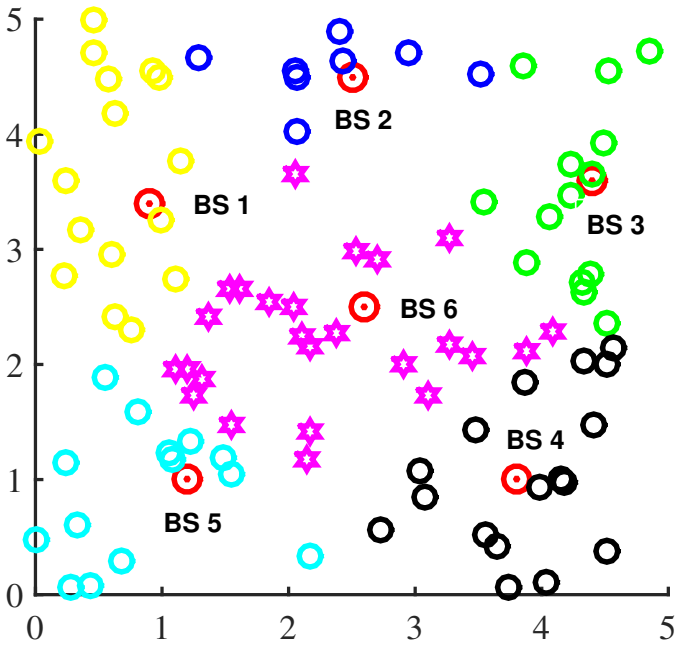

Figure 2.11 BS with the largest H_j assists the BS with the smallest H_j.

BS 6 associates one more user from BS 1 (pointed out by the arrow), as shown in Figure 2.12. BS 1 is the BS with the second smallest H_j around BS 6. Since the latency ratio of BS 6 reaches its predefined threshold μ_{thres}, it stops serving more users from surrounding BSs because the higher latency ratio, which exceeds μ_{thres}, will lead to "penalty" in terms of losing profit. BS 2 is with the second largest H_j in this macro cell because it has a small $\mu_j(t)$. BS 1 is the BS with the smallest H_j around BS 2 (among BS 1, 6 and 3). Hence, as shown in Figure 2.13, BS 2 absorbs some users from BS 1 to reduce the energy consumption and/or alliterate traffic congestion for BS 1 in order to increase profit for this macro cell. The blue

stars stand for the users associated with BS 2 after modifying user association. Then, the BS with the third largest H_j repeats this process to check whether it can help its surrounding BSs to gain the profit for this macro cell. Then, the fourth one repeats, and so on. For brevity, we just show the association modifications for the BS with the largest H_j and the BS with the second largest H_j.

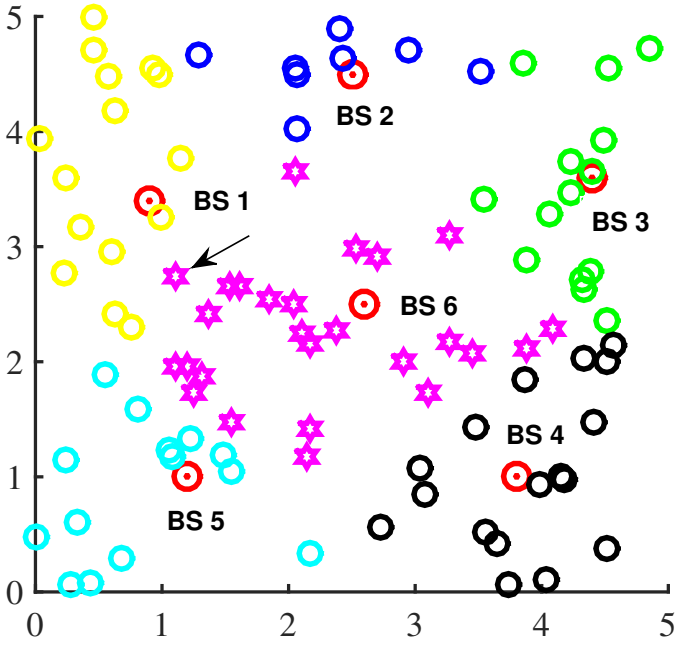

Figure 2.12 BS with the largest H_j assists the BS with the second smallest H_j.

In this work, we compare the performances of our proposed PDU heuristic algorithm, the Min-max Residual Green energy Ratio (RGR) algorithm [44], Profit User association Heuristic (PUH) algorithm [40] and the SSF scheme from different aspects and set them with the same simulation settings. Figure 2.14 shows the growth of traffic latency as the number of mobile users increases in the macro cell. In order to maximize the green energy utilization, the Min-max RGR algorithm always forces the BS with the most residual green energy to serve a large number of users and does not consider the latency issue in the network. Hence, its overall traffic latency ratio is the highest among the four algorithms. Since SSF does not change BS coverage or modify the user associations based on the traffic, its traffic latency simply goes up with the

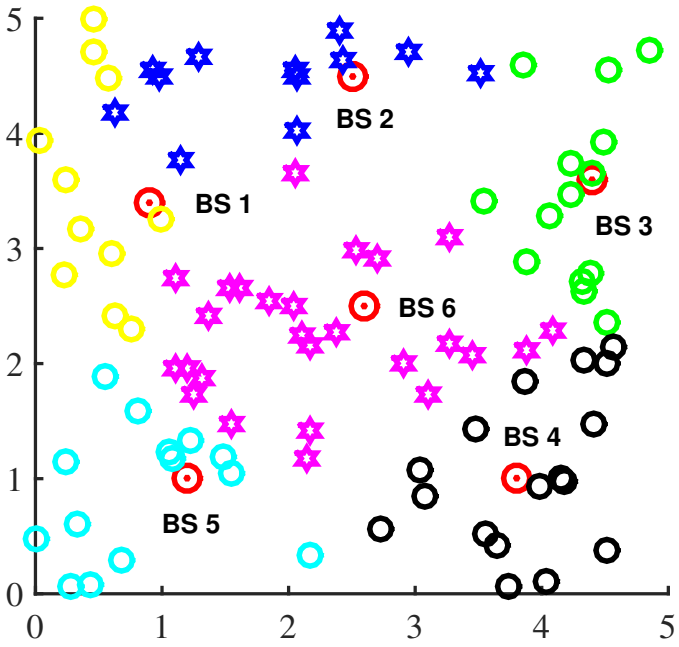

Figure 2.13 BS with the second largest H_j assists its surrounding BS with the smallest H_j.

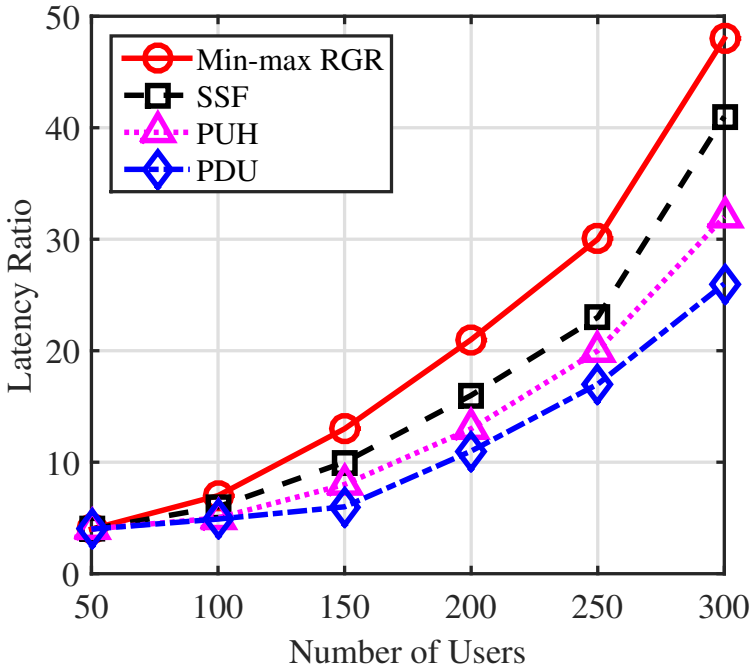

Figure 2.14 Traffic latency ratio vs. number of mobile users.

increase of users. PUH intends to maximize profit in the network but it does not have a latency feedback mechanism in the algorithm, i.e., a congested BS with less residual

green energy will always offload its users to the adjacent BS with abundant green energy, but this may lead to new traffic congestion at its adjacent BS. Our proposed PDU algorithm has the latency feedback mechanism in the algorithm. A BS stops absorbing more users when its traffic latency ratio reaches the predefined latency ratio threshold μ_{thres}, even if it still has surplus residual green energy. Therefore, the PDU algorithm will not cause new local traffic congestion, and so the overall traffic latency ratio does not grow rapidly.

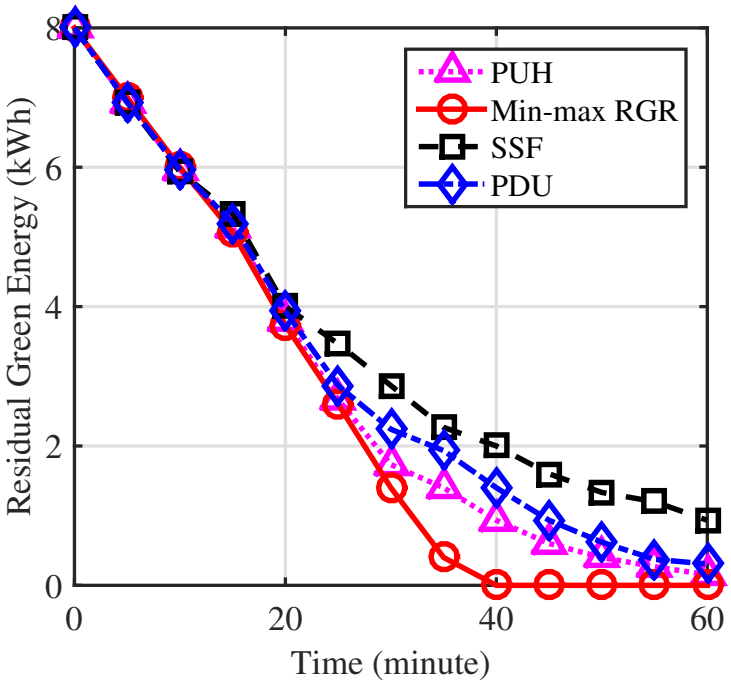

Figure 2.15 Total residual green energy in a battery cycle.

Figure 2.15 shows the total residual green energy in the discharging batteries in a macro cell of these four algorithms for serving 200 mobile users during one battery cycle. Since SSF does not associate users based on the green energy, it retains the most green energy at the end of the battery cycle among the four algorithms, i.e., the green energy is not fully used. Min-max RGR maximizes the green energy utilization, and so it exhausts green energy earlier than the other three algorithms. As aforementioned, PUH does not have latency feedback mechanism in the algorithm, a BS with relatively abundant residual green energy will keep absorbing mobile users from the surrounding

BSs with insufficient residual green energy as long as the profit increases. Thus, its amount of residual green energy is close to that of the Min-max RGR algorithm. The proposed PDU has the latency feedback mechanism in the algorithm. Even through a BS still has some surplus residual green energy, when its traffic latency ratio reaches the predefined latency ratio μ_{thres}, it will stop absorbing more users from surrounding BSs to avoid instigating new traffic congestion. Therefore, its green energy utilization is less than that of PUH.

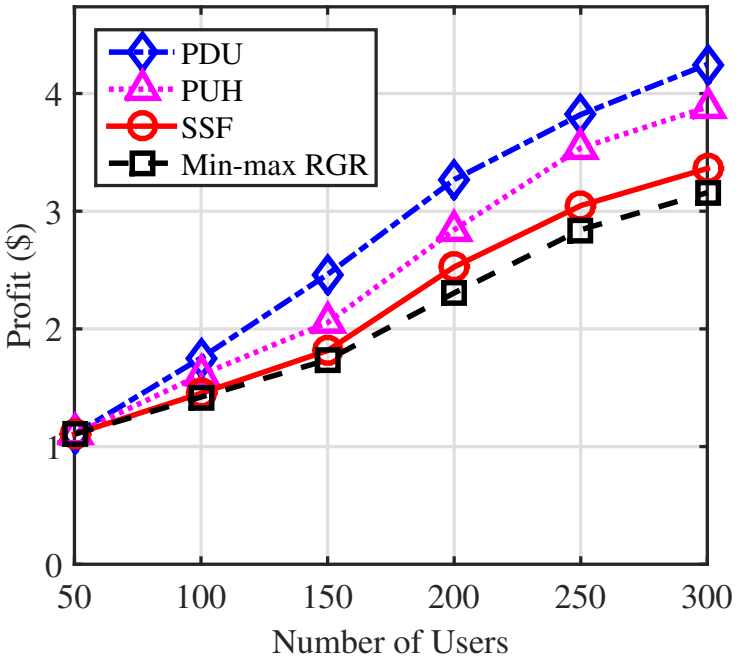

Figure 2.16 Profit vs. number of mobile users.

Figure 2.16 shows the total profit increasing trend versus the number of mobile users in this macro cell; we apply the same pricing model to the comparison algorithms. Since SSF does not modify user-BS association based on the traffic and green energy, its profit grows with the increase of users. Min-max RGR can reduce on-grid energy consumption by maximizing the green energy utilization, i.e., the BS with more residual green energy will associate more mobile users, thus inducing some local traffic congestions that leads to "penalties" based on the pricing model. Since the PUH algorithm does not have latency feedback mechanism in the algorithm, local

traffic congestions will also cause "penalties" in the overall profit. In our proposed PDU heuristic algorithm, the BSs with larger H_j are the candidates to serve more users; when their traffic latency ratios reach the predefined latency ratio μ_{thres}, they will not bring more traffic into their downlink transmission. This algorithm jointly considers the traffic delivery latency and green energy utilization to balances traffic load among BSs while making good use of green energy; the network provider profits from both aspects. The achieved profit of the PDU heuristic algorithm is slightly higher than that of the PUH algorithm. Even though the green energy utilization is not higher than that of the PUH algorithm, the PDU heuristic algorithm incorporates the importance of the network provider in provisioning users with the promised QoS.

2.4 Summary

In this chapter, we have proposed the dual-battery architecture to harvest and manage green energy in the cellular network. By installing dual-battery, the amount of available green energy at each BS is known and accurate for every time period. We have also proposed the profit-driven user association scheme to jointly consider the green energy utilization and traffic delivery latency in the network to maximize the profits of the network providers.

CHAPTER 3

GREEN D2D COMMUNICATIONS

As aforementioned, a large number of IoT applications are emerging. For example, in the residential area, smart homes can be facilitated by IoT via home appliance automation control. In hospitals, various medical facilities can sense and cooperate to provide prompt patient services. In factories and farms, instruments can collaborate with each other to enhance the performance and efficiency of factory and farm operations. IoT also enables vehicle-to-vehicle and vehicle-to-person communications to improve traffic management and transportation safety. There are many other IoT application scenarios, such as context aware smart space, proximal files sharing, proximal social networking and fog computing.

It is imperative to decouple D2D communications from the occupied cellular spectrum to facilitate ubiquitous, seamless and quality services required for IoT. By leveraging the overlay spectrum sharing approach, D2D and cellular communications are to be accommodated on separated spectra to avoid the mutual interference. This is beneficial to both cellular and D2D users. There is a constant demand for new spectral bands to boost the new generation of communications [7], [1]. In fact, on July 14, 2016, FCC voted to open up almost 11 GHz of spectrum for wireless communications [3]. Besides utilizing licensed spectrum, portions of unlicensed spectrum have been proposed to be integrated into Long-Term Evolution (LTE) cellular networks to facilitate IoT and D2D communications [65], [53]. Therefore, we assume additional spectrum will be dedicated for D2D communications in realizing IoT.

In this work (the detail information can be referred to [39]), consider a heterogeneous cellular network with multiple macro BSs and pico BSs (pico BSs

act as relay BSs) as shown in Figure 3.1. The macro BSs are evenly placed according to a hexagonal grid. In this work, the spectrum reuse factor for cellular frequency planning is 1/3, which implies that 3 adjacent macrocells, for example, Cells 1, 2 and 3, cannot utilize the same spectral band. Thus, two adjacent macrocells will have no interference [63], [20]. We adopt the overlay spectrum sharing approach to facilitate D2D communications, and there is no interference between D2D and cellular network. All the macro BSs and relay BSs in this network are synchronized and coordinated. Assume the relay BSs within a macrocell can cooperatively cover this macrocell completely, and so any device within this macrocell can be served by the relay BSs.

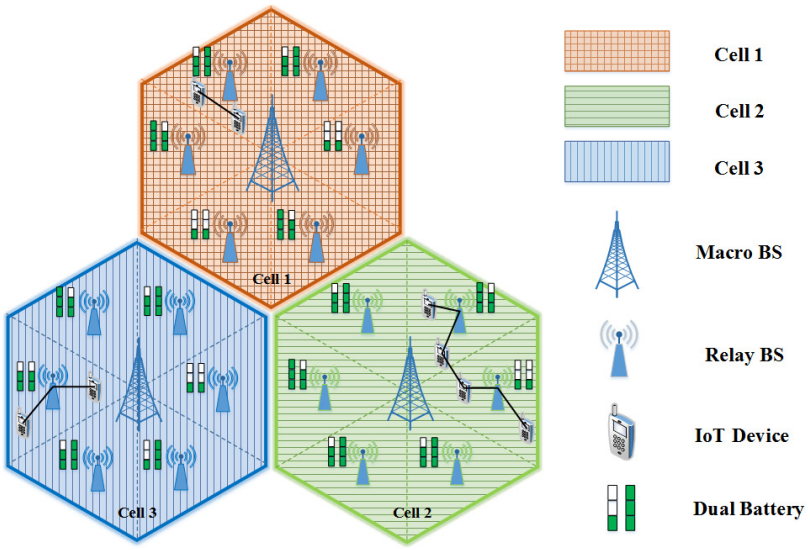

Figure 3.1 Framework of green relay assisted D2D communications with dual-battery system in a heterogeneous cellular network.

3.1 System Model

3.1.1 Direct D2D Communications Group

For each picocell, the channel state information (CSI) between the devices, and that between the devices and the relay BS are assumed known by the relay BS [63], [62]. CSI includes multiple channel state factors, such as path loss, shadowing and fading.

According to CSI in every time slot, we partition the devices within a picocell into two groups. If the channel state in a source-destination (SD) device pair is better than the channel state between the source device and the relay BS, this SD pair is classified into the direct D2D group, in which the source device can directly transmit data to the destination device. As shown in Figure 3.2, the solid line represents the direct D2D transmission.

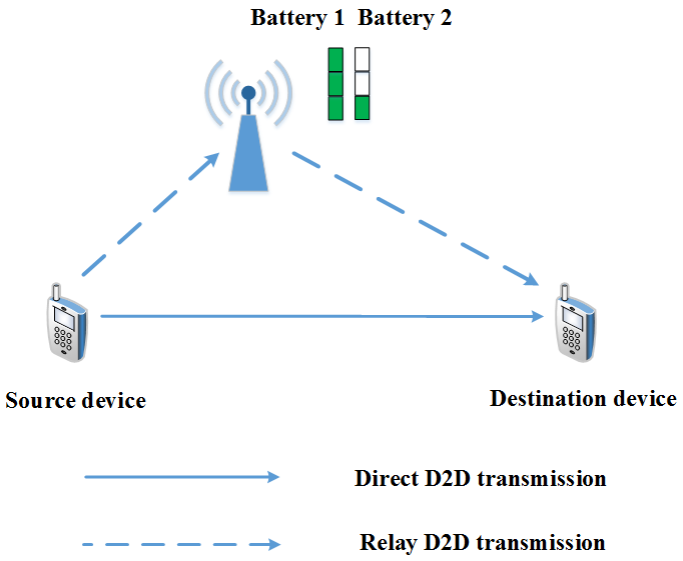

Figure 3.2 Direct and relay D2D communications.

Let M be the number of SD pairs in the direct D2D group under the coverage of a particular relay BS j; denote $S_{Direct} = (s_1, s_2, ..., s_m)$ and $D_{Direct} = (d_1, d_2, ..., d_m)$ as the source and destination devices in this group, respectively. Single-carrier frequency division multiple access (SC-FDMA) is adopted in the transmission between devices [45]. So, there is no interference within a picocell. Different picocells carve up and utilize all the orthogonal channels of this macrocell [37]. Hence, there is no interference between the picocells within the same macrocell. As aforementioned, there is no inter-macrocell interference, and hence, the transmission data rate for the mth SD

pair is

$$C_{m,j}^{SD} = W_{m,j}^{S} log_2(1 + \frac{P_{m,j}^{S} h_{m,j}^{SD}}{N_0 W_{m,j}^{S}}). \tag{3.1}$$

Here, $P_{m,j}^{S}$ is the transmission power of the mth source device in picocell j, $h_{m,j}^{SD}$ the channel gain between the mth source and destination device in picocell j, N_0 the power spectral density of additive white Gaussian noise (AWGN), and $W_{m,j}^{S}$ the bandwidth allocated to the mth SD pair in the jth picocell.

3.1.2 Relay Assisted Dual-hop D2D Communications Group

According to CSI, if the channel state between the source device and the relay BS is better than or equal to that in an SD pair, this SD pair is classified into the relay assisted dual-hop D2D group (for simplicity, relay D2D group), because the channel state favors the transmission from the source device to the relay BS. The relay BS can relay the information for the source device to its corresponding destination device with an equal or higher data rate. In this case, the source device saves energy by sending data to the relay BS, instead of being constrained from transmitting to the destination device in a poor quality link. As shown in Figure 3.2, the dash line refers to the relay D2D transmission.

Let N be the number of SD pairs in the relay D2D group under the coverage of the relay BS j, and $S_{Relay} = (s_1^{'}, s_2^{'}, ..., s_n^{'})$ and $D_{Relay} = (d_1^{'}, d_2^{'}, ..., d_n^{'})$ denote the sets of source and destination devices, respectively. Similarly, without interference, the transmission data rate from the nth source device to relay BS (SR link) is

$$C_{n,j}^{SR} = W_{n,j}^{S} log_2(1 + \frac{P_{n,j}^{S} h_{n,j}^{SR}}{N_0 W_{n,j}^{S}}). \tag{3.2}$$

Here, $P_{n,j}^{S}$ is the transmission power of the nth source device in the jth picocell. $h_{n,j}^{SR}$ is the channel gain between the nth source device and the relay BS j. $W_{n,j}^{S}$ is the bandwidth allocated to the nth source device.

The transmission data rate for the relay BS for serving the nth destination device (RD link) is

$$C_{n,j}^{RD} = W_{n,j}^{R} log_2(1 + \frac{P_{n,j}^{R} h_{n,j}^{RD}}{N_0 W_{n,j}^{R}}). \tag{3.3}$$

Here, $P_{n,j}^{R}$ is the transmission power of the jth relay BS for serving the nth destination device. $h_{n,j}^{RD}$ is the channel gain between the relay BS j and the nth destination device. $W_{n,j}^{R}$ is the bandwidth allocated for serving the nth destination device.

For the relay assisted dual-hop D2D communications, the nth source device sends the data to the relay BS in the first time unit, and then the relay BS sends the received data to the nth destination device in the second time unit [69], and hence the effective data rate of this SD pair is

$$C_{n,j}^{SD} = \frac{1}{2} \min \left\{ C_{n,j}^{SR}, C_{n,j}^{RD} \right\}. \tag{3.4}$$

3.2 Network Resource Allocation Optimization

Our proposed architecture facilitates not only intra-picocell D2D communications, but also multi-hop inter-pico/macrocell D2D communications by sharing the routing information among pico/macro BSs. The source device will first inquire the IP/MAC addresses of the destination device at the local relay BS, and if the destination device is in the same picocell, the relay BS will establish the intra-picocell D2D transmission for this SD pair; otherwise, the local relay BS will schedule a routing path for this source device, i.e., the relay BS first relays the information to an intermediate device located at its coverage boundary, and then this intermediate device will be guided to associate with the neighboring relay BS in the next time slot, and forward the information to that neighboring relay BS or to other device guided by that neighboring relay BS. The information being delivered among different picocells or macrocells is eventually delivered to the destination device.

Within the coverage of a relay BS, no matter whether the transmission is a complete transmission of intra-picocell D2D communications or a partial transmission of multi-hop inter-pico/macrocell transmission, there always involves one SD pair under the coverage of a relay BS. Therefore, we perform the resource allocation optimization for the two groups of SD pairs within the relay BSs of each macrocell in each time slot.

3.2.1 Resource Allocation for the Direct D2D Group

Consider there are J picocells in one macrocell. $P^S_{m,j}$ is the transmission power of the mth source device in the direct D2D group in the jth picocell. Different types of devices have different transmission power $P^S_{m,j}$, and for the same source device its $P^S_{m,j}$ can also be different in different time slots. In this work, we assume in each time slot, $P^S_{m,j}$ of each device is fixed and known by the relay BS through the control link before the transmission [21]. Denote $C^{SD}_{m\_req,j}$ as the required data rate of the IoT application of the mth SD pair; $C^{SD}_{m\_req,j}$ can be different in different time slots for different SD pairs; assume they are fixed and known by the relay BS for each time slot. The channel gain $h^{SD}_{m,j}$ and noise power spectral density N_0 in Equation 3.1 remain constant within each time slot. The resource allocation scheme for the devices in the direct D2D group is to assign the proper bandwidth for each SD pair's data rate $C^{SD}_{m,j}$ to reach its required service data rate $C^{SD}_{m\_req,j}$, i.e.,

$$C^{SD}_{m,j} = C^{SD}_{m\_req,j} = W^S_{m,j} log_2(1 + \frac{P^S_{m,j} h^{SD}_{m,j}}{N_0 W^S_{m,j}}). \tag{3.5}$$

Here, $W^S_{m,j}$ is the only variable in Equation 3.5. According to Shannon's Theorem [56], for a fixed $P^S_{m,j}$, by increasing its transmission bandwidth $W^S_{m,j}$, the data rate will be increased accordingly. Also, note that $C^{SD}_{m,j}$ is a concave increasing function of $W^S_{m,j}$ for a fixed $P^S_{m,j}$ [12]; by increasing $W^S_{m,j}$, the transmission data rate $C^{SD}_{m,j}$ will be increased. Therefore, properly allocating bandwidth to each SD pair in the direct

D2D group can facilitate the data rate to satisfy their application required service data rate. The occupied bandwidth for the direct D2D group in the jth picocell is $W_{Direct,j} = \sum_{m=1}^{M} W_{m,j}^{S}$. Thus, the occupied bandwidth for the direct D2D group in this macrocell is $W_{Direct} = \sum_{j=1}^{J} W_{Direct,j}$.

3.2.2 Resource Allocation for the Relay D2D Group

Suppose the total available spectrum bandwidth for IoT D2D communications in a macrocell is W_{D2D}. We have obtained the occupied bandwidth for the direct D2D group in this macrocell as W_{Direct}, and so the remaining bandwidth for the relay D2D group is $W_{Relay} = W_{D2D} - W_{Direct}$. The transmission of the relay D2D group concurs with that of the direct D2D group within the same time slot. In order to schedule the transmission and optimize the resource allocation for the relay D2D group, the time slot for the relay D2D transmission is further evenly divided into two sub-time slots, as shown in Figure 3.3. The first sub-time slot is for the source device to the relay BS (SR link) transmission; the second sub-time slot is for the relay BS to the destination device (RD link) transmission. The available bandwidth for the relay D2D group W_{Relay} is fully used in the first sub-time slot, and then fully used in the second sub-time slot again.

First Sub-time Slot Resource Allocation Optimization Again, consider J picocells in a macrocell. For all the devices in the relay D2D groups of these J picocells, in the first sub-time slot, each relay BS will allocate the bandwidth to each source device within its own picocell coverage. The optimization objective is to maximize the overall data rates from all the source devices to their corresponding relay BSs, i.e., maximizing the overall data rates at the SR links for all these J picocells, while guaranteeing half of the data rate of each SR link $\frac{1}{2}C_{n,j}^{SR}$ not to be lower than the application required data rate of each SD pair $C_{n\_req,j}^{SD}$, according to Equation 3.4. Here, $C_{n\_req,j}^{SD}$ is the required data rate by the IoT application of the nth SD pair;

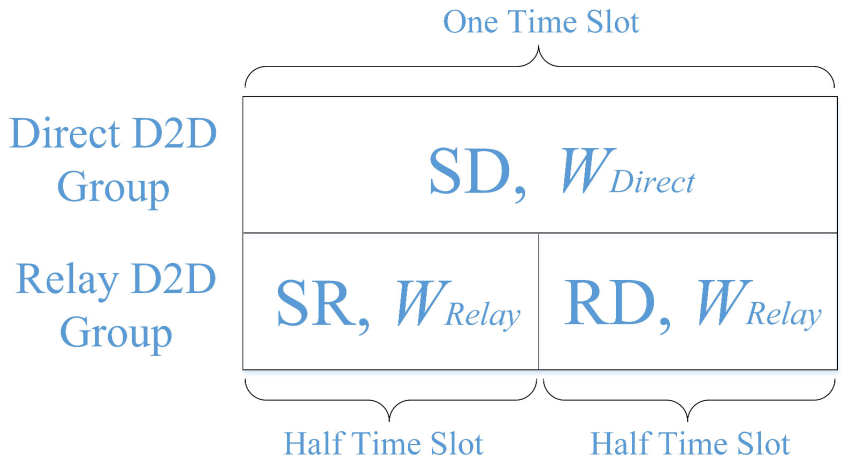

Figure 3.3 Resource allocation framework within one time slot.

$C^{SD}_{n\_req,j}$ can be different in different time slots for different SD pairs; $C^{SD}_{n\_req,j}$ is assumed fixed and known by the relay BS for each time slot. The rationale of this objective is to maximize the overall data rate for all the source devices and at the same time reduce their energy consumption. From the perspective of a device, transmitting the same amount of data at a higher data rate incurs less transmission time. Less time multiplied by the fixed transmission power indicates less energy consumption in the device. The objective for the first sub-time slot is to maximize the sum rate of all the source devices, i.e.,

$$\max_{\{W^S_{n,j}\}} \sum_{j=1}^{J}\sum_{n=1}^{N} C^{SR}_{n,j} \tag{3.6}$$

$$s.t. \quad C^{SD}_{n\_req,j} \leq \frac{1}{2} C^{SR}_{n,j} \tag{3.7}$$

$$\sum_{j=1}^{J}\sum_{n=1}^{N} W^S_{n,j} \leq W_{Relay} \tag{3.8}$$

$$0 < W^S_{n,j}. \tag{3.9}$$

Here, Equation 3.7 constrains half of the data rate at the SR link not to be less than the data rate required by the nth SD pair. Equation 3.8 implies that the total

allocated bandwidth for the source devices should be less than or equal to the available bandwidth for the relay D2D group W_{Relay} in this macrocell. $W^S_{n,j}$ is the bandwidth to be allocated to the nth source device in the jth picocell. From Equation 3.2, it can be seen that $C^{SR}_{n,j}$ is a concave increasing function of $W^S_{n,j}$. The summation of concave functions, Equation 3.6, is still concave [12]. Hence, this optimization problem can be solved efficiently. Each $W^S_{n,j}$ will lead to a corresponding data rate $C^{SR}_{n,j}$ for each SR link. Therefore, the data rates of the SR links are known and fixed for the resource allocation optimization for the subsequent second sub-time slot.

Second Sub-time Slot Resource Allocation Optimization In the first sub-time slot, we have obtained the optimal data rate $C^{SR}_{n,j}$ for each source device, which has been guaranteed to be $\frac{1}{2}C^{SR}_{n,j} \geq C^{SD}_{n\_req,j}$ already. According to Equation 3.4, the minimal of $C^{SR}_{n,j}$ and $C^{RD}_{n,j}$ determines the effective data rate between the source and destination device, because one of them will be the bottleneck. Thus, in the second sub-time slot resource allocation optimization, we should guarantee $C^{RD}_{n,j} \geq C^{SR}_{n,j}$ to achieve the IoT application required data rate. By leveraging the relay BS transmission power, the relay BS can enable the RD link to achieve a higher data rate than that of the SR link because the relay BS has much higher transmission power than the mobile device. Therefore, the optimization objective in the second sub-time slot is to minimize all the picocell relay BSs' transmission power for serving all the destination devices in the relay D2D groups in this macrocell, while guaranteeing $C^{RD}_{n,j} \geq C^{SR}_{n,j}$. It is desired to minimize all the relay BSs' energy consumption, no matter whether the relay BSs are powered by green energy or on-grid energy. The objective for the second sub-time slot resource allocation optimization is to minimize

the transmission power of the relay BSs, i.e.,

$$\min_{\{P^R_{n,j}, W^R_{n,j}\}} \sum_{j=1}^{J} \sum_{n=1}^{N} P^R_{n,j} \tag{3.10}$$

$$s.t. \;\; C^{SR}_{n,j} \leq C^{RD}_{n,j} \tag{3.11}$$

$$\sum_{j=1}^{J} \sum_{n=1}^{N} W^R_{n,j} \leq W_{Relay} \tag{3.12}$$

$$\sum_{n=1}^{N} P^R_{n,j} \leq P_{Total,j} \tag{3.13}$$

$$0 < W^R_{n,j} \tag{3.14}$$

$$0 < P^R_{n,j}. \tag{3.15}$$

Here, Equation 3.11 guarantees the data rate of the RD link not to be less than the data rate of the SR link. $W^R_{n,j}$ is the bandwidth for serving the nth destination device in the jth picocell. Equation 3.12 implies the total allocated bandwidth for serving the destination devices not to exceed the available W_{Relay} in this macrocell. $P^R_{n,j}$ is the relay BS transmission power for serving the nth destination device. Owing to the hardware limitation, $P_{Total,j}$ is the maximum transmission power of the relay BS j; Equation 3.13 imposes the total transmission power for serving the destination devices not to exceed its maximum transmission power $P_{Total,j}$. It can be proved that this optimization problem is a convex problem, and hence its optimal solution can be obtained efficiently.

Proposition 4. *The second sub-time slot resource allocation optimization problem is a convex problem.*

Proof. According to Equation 3.13, the transmission power at the jth relay BS for serving the nth destination device $P^R_{n,j}$ can be expressed as

$$P^R_{n,j} = (2^{\frac{C^{RD}_{n,j}}{W^R_{n,j}}} - 1) \cdot \frac{N_0 W^R_{n,j}}{h^{RD}_{n,j}}. \tag{3.16}$$

Hence, the objective function Equation 3.10 and its constraints can be re-written as

$$\min_{\{W^R_{n,j}, C^{RD}_{n,j}\}} \sum_{j=1}^{J} \sum_{n=1}^{N} (2^{\frac{C^{RD}_{n,j}}{W^R_{n,j}}} - 1) \cdot \frac{N_0 W^R_{n,j}}{h^{RD}_{n,j}} \tag{3.17}$$

$$s.t. \quad C^{SR}_{n,j} \leq C^{RD}_{n,j} \tag{3.18}$$

$$\sum_{j=1}^{J} \sum_{n=1}^{N} W^R_{n,j} \leq W_{Relay} \tag{3.19}$$

$$\sum_{n=1}^{N} P^R_{n,j} \leq P_{Total,j} \tag{3.20}$$

$$0 < W^R_{n,j} \tag{3.21}$$

$$0 < C^{RD}_{n,j}. \tag{3.22}$$

Here, $W^R_{n,j}$ and $C^{RD}_{n,j}$ are the only variables in Equation 3.17; the values of other notations are all given. By calculating the second-order derivatives, the Hessian matrix of Equation 3.16 is positive semidefinite. That is, Equation 3.16 is a convex function [12]. The summation of convex functions, Equation 3.17, is still convex [12]. The inequality constraints (Equations 3.18-3.20) are also convex. Hence, this optimization problem is convex. □

3.2.3 Green Energy Balancing Optimization with Dual-Battery

By installing dual-batteries at relay BSs, the amount of available green energy for each time period is known and accurate. We consider solar energy harvested from solar panels at the relay BSs as the green energy source in this work though other renewal sources can be equally adopted. We denote T as the battery cycle and T is selected to be an integer multiple of time slot τ. At the beginning of each battery cycle, the initial total available green energy in a battery of relay BS j is E^0_j, which was harvested in the previous battery cycle. E^0_j can be different in different battery cycles at the same or a different relay BS j, and has to be less than or equal to the full battery capacity. As time elapses during the battery cycle, the residual green energy

in the battery of relay BS j at the tth time slot is E_j^t. $0 \leqslant E_j^t \leqslant E_j^0$ constrains E_j^t to be between zero and the initial green energy E_j^0 stored in the battery. E_j^t at the relay BS j is updated for each time slot t. In Equation 3.10, we have obtained the energy consumption $\sum_{n=1}^{N} P_{n,j}^R$ for each relay BS of each time slot. Since this amount of energy is only consumed in every second sub-time slot, the energy consumption of relay BS j during the tth time slot can be expressed as

$$K_j^t = \sum\nolimits_{n=1}^{N} P_{n,j}^R \frac{\tau}{2} + P_j^{static}\tau, \tag{3.23}$$

and P_j^{static} is the static power consumption of BS j.

Based on our proposed architecture, the relay BSs are connected with each other not only by networking cables/fibers, but also connected by electric transmission lines for balancing residual green energy. Transferring green energy among local relay BSs is more efficient than delivering on-grid energy from a remote power plant, in terms of electricity transmission loss [50]. In every time slot, according to the energy consumption K_j^t of the relay BSs and the residual green energy E_j^t in their batteries, the green energy balancing execution policy adopts the guideline below. Guideline 1 is motivated by the following intuition. When some relay BSs do not have sufficient green energy to accommodate their communication workloads, the other relay BSs with abundant green energy may transmit electricity to supplement those relay BSs with insufficient green energy. Thus, those relay BSs can first temporally utilize green energy, instead of consuming on-grid energy immediately. This guideline maximizes the utilization of the available green energy in a macrocell and furthest reduces on-grid energy consumption.

Guideline 1.

1) When all the relay BSs have sufficient residual green energy to supplement their workloads demanded energy in each time slot, i.e., $E_j^t \geq K_j^t$, the relay BSs directly drain the energy from their own batteries.

2) Once one relay BS has insufficient residual green energy to accommodate its communication workload in the current time slot, i.e., $E_j^t < K_j^t$, then this relay BS is classified into a set, $\boldsymbol{S_1}$. The rest of relay BSs with sufficient residual green energy are classified into the other set, $\boldsymbol{S_2}$, and each relay BS in this set is indexed by i. According to the amount of their residual green energy, the relay BSs in $\boldsymbol{S_2}$ will transmit their electricity to the relay BS in $\boldsymbol{S_1}$, to supplement the shortage of green energy.

3) As more relay BSs exhaust their green energy, the number of relay BSs in $\boldsymbol{S_1}$ increases. Relay BSs in $\boldsymbol{S_2}$ continuously transmit electricity to relay BSs in $\boldsymbol{S_1}$. When the total green energy shortage in $\boldsymbol{S_1}$, $\sum_{j \in \boldsymbol{S_1}} (K_j^t - E_j^t)$, is larger than the total surplus green energy in $\boldsymbol{S_2}$, $\sum_{i \in \boldsymbol{S_2}} (E_i^t - K_i^t)$, the relay BSs in $\boldsymbol{S_2}$ only transmit green energy to those in a subset of $\boldsymbol{S_1}$, i.e., $\boldsymbol{S_1'} \subset \boldsymbol{S_1}$, with $\sum_{j \in \boldsymbol{S_1'}} (K_j^t - E_j^t) < \sum_{i \in \boldsymbol{S_2}} (E_i^t - K_i^t)$.

4) When all the relay BSs belong to $\boldsymbol{S_1}$, the relay BSs stop transmitting electricity between each other.

In practice, the electric power transmission efficiencies of the electric transmission lines between each pair of relay BSs are different. Transmitting electricity through the electric transmission lines leads to some electricity loss. Here, our goal is to minimize the electricity loss when the electricity is transmitted among the relay BSs, i.e., maximizing the amount of effective electricity transmitted along the transmission lines. We will determine which relay BSs in $\boldsymbol{S_2}$ should transmit to which relay BSs in $\boldsymbol{S_1}$ or $\boldsymbol{S_1'}$ by how much electricity for the above Steps 2) and 3). Assume every two relay BSs in a macrocell are connected by an electric transmission line. We use i, j to denote two different relay BSs in a macrocell, respectively. Here, $i \in \boldsymbol{S_2}$ and $j \in \boldsymbol{S_1}$ or $\boldsymbol{S_1'}$. $\theta_{i,j}$ is the electric transmission line loss-rate between relay BS i and j. $0 < \theta_{i,j} < 1$ is assumed known in advance, according to the distance between the relay BSs and the material of the electric transmission line. A higher $\theta_{i,j}$ implies a larger electricity transmission loss, i.e., lower electricity transmission efficiency. $\delta_{i,j}$

represents the amount of electricity (green energy) to be transmitted from relay BS i to relay BS j. The objective is to minimize the amount of electricity transmission loss in this macrocell, and so the objective is to

$$\min_{\{\delta_{i,j}\}} \sum_{i \in \boldsymbol{S_2}, j \in \boldsymbol{S_1'}} \theta_{i,j} \delta_{i,j} \tag{3.24}$$

$$s.t. \sum_{i \in \boldsymbol{S_2}, j \in \boldsymbol{S_1'}} (1 - \theta_{i,j}) \delta_{i,j} = \sum_{j \in \boldsymbol{S_1'}} (K_j^t - E_j^t) \tag{3.25}$$

$$0 \leq \delta_{i,j} \leq E_i^t - K_i^t \tag{3.26}$$

$$0 < \theta_{i,j} < 1. \tag{3.27}$$

The left side term of Equation 3.25 is the effective amount of electricity transmitted from the relay BSs in $\boldsymbol{S_2}$ to those in $\boldsymbol{S_1'}$ in this macrocell, and the right side term of Equation 3.25 is the amount of energy requested from the relay BSs in $\boldsymbol{S_1'}$ to supplement their green energy shortage. The left side term equaling to the right side term means all the requested energy from $\boldsymbol{S_1'}$ is fulfilled by the relay BSs in $\boldsymbol{S_2}$. Equation 3.26 constrains $\delta_{i,j}$ to be between zero and the amount of surplus green energy of relay BS i at current time slot t. Since this green energy balancing problem is a linear programming problem and $\delta_{i,j}$ is the only variable, it can be solved efficiently. This green energy balancing optimization policy guarantees all the green energy harvested in this network to be fully utilized first, thus achieving the goal of furthest reducing the on-grid energy consumption.

3.2.4 Simulation Results

Simulations are set up as follows. One macrocell contains six picocells. The radius of this macrocell is $750m$. The picocell relay BSs are deployed uniformly within this macrocell, and their locations are fixed. The distribution of devices is generated by the Poisson point process (PPP) in this macrocell [34]. The distance-dependent channel model [63] is adopted in simulations. Within each time slot $\tau = 10ms$, the devices'

locations are fixed. Each device is arbitrarily assigned one level of transmission power, either $200mW$ or $300mW$; within each time slot, the transmission power of a source device is fixed. Within the coverage of each picocell, the pairing for the SD pairs is arbitrarily assigned. Also, the IoT application required data rate of each SD pair is arbitrarily assigned among 2Mbps, 6Mbps and 10Mbps; within each time slot, the required data rate is fixed. The total available bandwidth in a macrocell for D2D communications is 20MHz. The electric transmission line loss-rate $\theta_{i,j}$ between every two relay BSs are randomly generated between 5% and 10%, and fixed in the experiments.

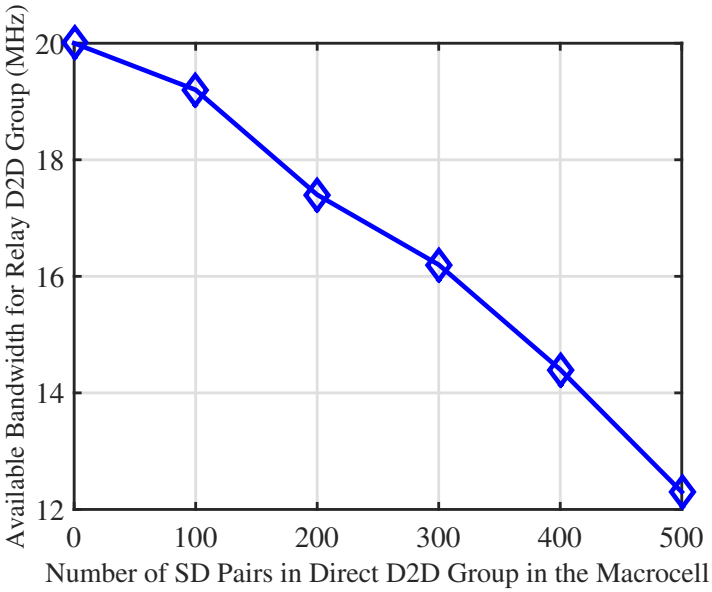

Figure 3.4 Average available bandwidth for relay D2D group.

Figure 3.4 shows the average available bandwidth for the relay D2D group versus the number of SD pairs in the direct D2D group in a macrocell. This figure presents the Monte Carlo result obtained from one thousand repeated experiments. In these experiments, we fix the total number of SD pairs as 1000 and record the number of SD pairs in the direct D2D group of this macrocell and the corresponding average available bandwidth for the relay D2D group. The decreasing line implies that the more SD pairs belong to the direct D2D group, the less available bandwidth for the

relay D2D group because we allocate the spectrum to the direct SD pairs first in executing our resource allocation method. In each experiment, as the number of SD pairs in the direct D2D group increases, the required bandwidth increases. As the total bandwidth for IoT D2D communications is fixed, the more bandwidth used by the direct D2D group, the less available bandwidth left for the relay D2D group. In theory, if all the SD pairs belong to the direct D2D group (owing to the proximity of SD devices with very good channel condition), then there will be no SD pairs in the relay D2D group and we can allocate all the spectrum for the direct D2D transmissions. If this is the case, our architecture achieves the pure and ideal D2D communications, i.e., all the SD pairs can directly communicate, and no energy is consumed at the relay BSs for relaying data.

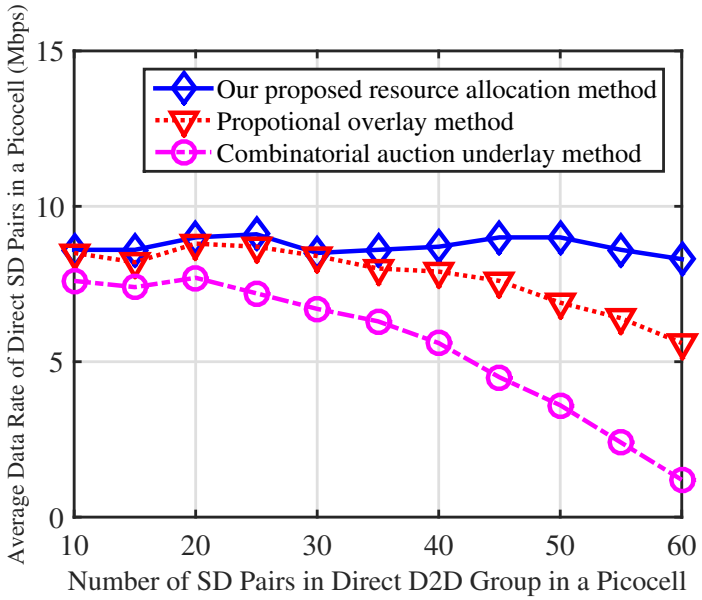

Figure 3.5 Average data rate of SD pairs in the direct D2D group.

Figure 3.5 shows the average data rate of the direct SD pairs in a picocell with different numbers of SD pairs in the direct D2D group. We randomly choose a picocell in the macrocell to observe the performance of different resource allocation methods on the average data rate with different numbers of direct SD pairs. The top blue curve with diamond marks nearly remains unchanged as the number of SD

pairs in the direct D2D group increases because our proposed resource allocation method allocates the spectrum to the direct D2D group first to fulfill their IoT applications required bandwidth. We serve the direct SD pair as the "preferred user", and the remaining spectrum is allocated for the relay D2D group. Since the average required data rate of different types of D2D devices in the network is stable, the blue curve keeps nearly unchanged. The red curve with triangle marks represents the performance of a comparison method [34], which partitions the cellular spectrum into two parts, one part for cellular usage and the other part for D2D usage. The red curve performs almost the same as our proposed method with a small number of D2D pairs, but it deteriorates when more SD pairs transmit because in their proportional overlay spectrum sharing method, D2D users share channels to transmit; when more D2D users start their transmissions, their data rates are affected by the co-channel interference. Thus, the decreasing rate of the red curve is determined by the spectrum partition factor in [34]. The purple curve with circular marks is the performance of another comparison method [63], which degrades rapidly because in their iterative combinatorial auction underlay spectrum sharing method, the D2D user has to adjust its transmission power in order to avoid harmful interference to the cellular users, but it receives the interference from other co-channel D2D users as well as cellular users.

Figure 3.6 shows the average data rate of the relay SD pairs and the relay BS transmission power versus the number of SD pairs in the relay D2D group in a picocell. As the number of relay SD pairs increases, the average data rate of the relay SD pair in this group decreases because when more relay SD pairs share the limited bandwidth left for the relay D2D group, the available bandwidth for facilitating individual transmissions is less. Meanwhile, as the number of SD pairs increases, the total relay BS transmission power for serving the destination devices also increases because more RD links are served by the relay BS.

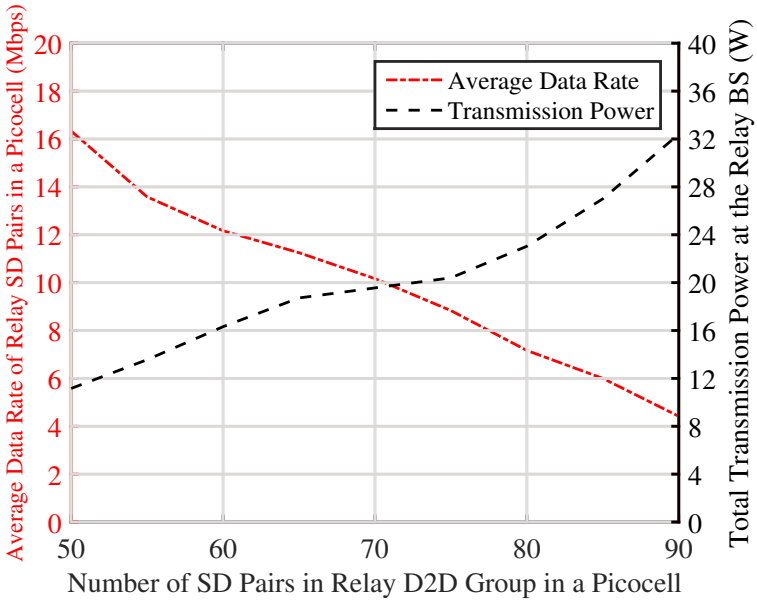

Figure 3.6 Average data rate and the relay BS total transmission power.

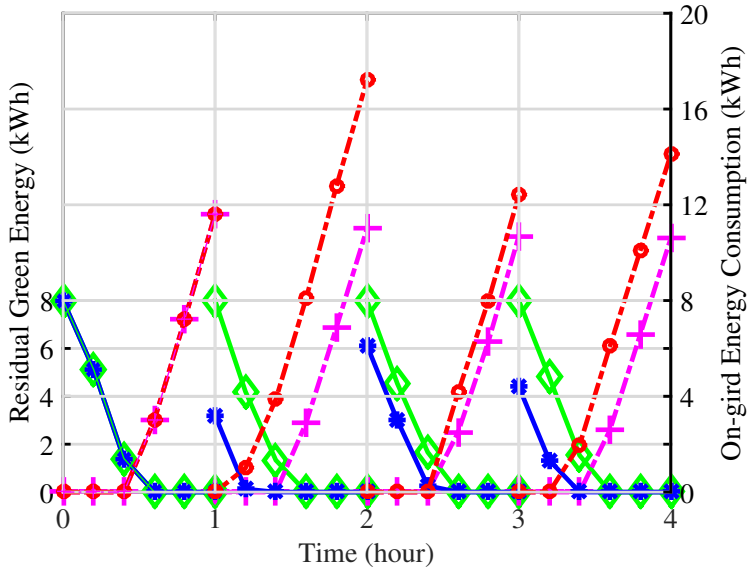

Figure 3.7 Performance comparison between the scenarios with single-battery and dual-battery.

Figure 3.7 shows the performance comparison between the scenarios with single-battery and dual-battery for serving 1500 SD pairs. In the single battery scenario, each relay BS is equipped with single battery. When the battery exhausts its green energy, it starts to harvest green energy (recharge); when the next battery cycle

begins, all the single batteries in the network start to power the relay BSs. In Figure 3.7, the blue curve with star marks and the red curve with circular marks indicate the residual green energy and on-grid energy consumption of the single battery scenario, respectively. The green curve with diamond marks and the purple curve with cross marks present the residual green energy and on-grid energy consumption of the dual-battery scenario, respectively. The two scenarios perform the same in the first battery cycle (Hour 1) because we initialize the same residual green energy for both scenarios and assume they experience the same communications workload. In the beginning of the second battery cycle (Hour 2), the single battery scenario's total harvested green energy is less than that in the dual batteries scenario because in the single battery scenario, in Hour 1, the single battery first spends some time to power the relay BS to exhaust its green energy, then turns into the recharging mode to harvest green energy. Its green energy harvesting (recharging) time is less than a full battery cycle. In comparison, in the dual-battery scenario, the two batteries alternately harvest green energy and power the relay BS, and therefore, when the first battery cycle ends, the second battery is well recharged by harvesting green energy; its harvested green energy is more than that in the single battery scenario. In the single battery scenario, less harvested green energy is exhausted quicker in each battery cycle; less portion of time utilizing green energy implies more on-grid energy to be supplementarily consumed.

3.3 Summary

A resource allocation scheme has been proposed in this chapter to facilitate green D2D communications such that in each macrocell, the required data rates of the SD pairs of IoT applications are satisfied and all the relay BSs' overall communication energy consumption is minimized. The utilization of green energy is maximized by balancing the residual green energy among the relay BSs, thus achieving the goal of furtherest saving on-gird energy.

CHAPTER 4

GREEN DEVICES

Global grandiose IoT implementations inevitably induce an unprecedented huge amount of energy consumption for powering IoT devices. IoT devices are predicted to be the leading energy guzzler in Information and Communications Technology by 2020 [49]; it has also been estimated that the global energy consumption of IoT edge devices approaches 46TWh by 2025, which is equal to Portugal's entire annual electricity consumption in the year of 2015 [49]. With the awareness of the depletion of brown energy sources on earth and the potential harmful environmental impacts caused by carbon emissions, it is essential to leverage green (renewable) energy to power IoT devices, in line with global environment-friendly and sustainable development of modern society.

Energy-constrained mobile IoT devices are required to be periodically tethered to the electric sockets (grid) cumbersomely for battery charging. The charging-cord (or even charging-pad) is the last barrier for mobile IoT devices to attain true "wireless" and convenience in modern life. Replacing batteries of IoT devices may be an alternative way to maintain operations, but usually incurs high costs and is inconvenient, hazardous, or even impossible (e.g., sensors embedded in human bodies or inside building structures). Intuitively, it is desirable to enable IoT devices with the green energy harvesting and wireless charging capabilities to realize their greening, independence and self-sustainability.

In this work (the detail information can be referred to [42]), we envision three steps to revolutionize and actualize green IoT. In Step 1, IoT devices can be self-powered by harvesting ambient energy, and we propose dual-battery green energy harvesting architecture for IoT devices. When the harvested ambient green energy in

Step 1 is insufficient to support IoT devices, in Step 2, nearby green pico base stations (PBSs) and femto base stations (FBSs) will leverage green energy to intentionally wirelessly charge the outdoor and indoor IoT devices by radio frequency (RF) waves. In the rest of this chapter, a BS is generally referred to as a PBS or a FBS. These green BSs are equipped with solar panels, wind turbines and dual-batteries to harvest green energy. Even though the wireless charging efficiency is relatively low, the BSs can keep emitting RF energy for a long time to charge the surrounding IoT devices; even though the BSs will consume a large amount of energy in this step, the energy sources of these BSs are green. As both the amount of harvested green energy and that to be wirelessly transferred at BSs exhibit spatial and temporal diversities, Step 3 is to balance green energy among the BSs to allow more BSs to leverage green energy. The latter step reinforces the former one to ensure the availability of green energy. The proposed innovation and energy flow for greening IoT is depicted and summarized in Figure 4.1.

The rest of this chapter is organized as follows. In Section 4.1, we first introduce some ambient green energy sources and propose dual-battery green energy harvesting architecture for IoT devices. Section 4.2 elaborates on a number of the latest technological breakthroughs in improving the wireless charging efficiency and realizing green energy wireless charging, while highlighting the corresponding key challenges and research directions. In order to further ensure the availability of green energy at individual BSs, cooperative green energy wireless charging and wired green energy balancing are proposed in Section 4.3. A summary is presented in Section 4.4.

4.1 Ambient Energy Harvesting for Green IoT

According to Energy Conservation Law, energy can neither be created nor destroyed; rather, it transforms from one form to another [54]. In the physical world, various ambient energies are "embedded" in the environment in different forms. They

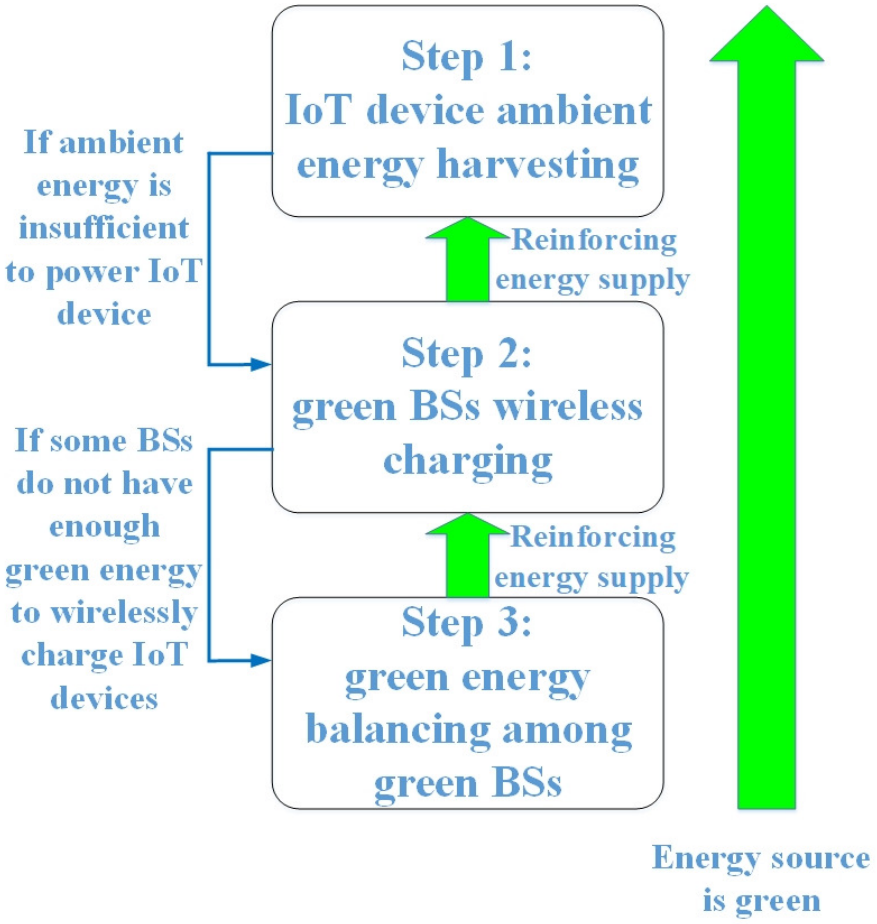

Figure 4.1 Framework for greening IoT.

are subsidiary products of natural phenomena or human activities, i.e., are not generated by intentionally consuming other additional brown energy, and thus they are "free" and "green". The significant concept of ambient energy harvesting is that the energy harvesting techniques should be wisely adopted according to the IoT devices' particular circumstances. In this section, we first list three typical ambient energies commonly present in our daily lives and the corresponding energy harvesting scenarios. Dual-battery green energy harvesting architecture is then proposed for IoT devices.

4.1.1 Ambient Energies and Harvesting

Piezoelectric: Electrical energy is converted from mechanical energy by straining a piezoelectric material. The straining of a piezoelectric material produces an electric field and consequently a voltage drop proportional to the stress applied.

Every footstep onto an electric shoe (monitoring human health) can generate electricity spontaneously. Human motion has been studied to power IoT devices [18]. Roadside monitoring sensors and smart traffic lights can leverage the vibration generated by vehicles running over the roads. To send or receive an important message via a smartphone with depleted energy, one may shake the smartphone and thus power it to do so.

Thermoelectric: The thermoelectric effect refers to a temperature gradient in a conducting material that leads to the diffusion of electric charge carriers. Thus, a voltage difference is created by the flow of charge carriers between the hot and cold regions.

IoT devices can be designed to harvest thermal energy in thermal environments to support their IoT functionalities [61]. A cup of hot coffee can potentially power its surrounding IoT devices.

Photovoltaic: By leveraging the photovoltaic effect, electricity is generated by converting the light shone onto semiconducting materials. A typical photovoltaic system deploys a number of solar cells, which convert the light into electrical energy.

Apparently, outdoor IoT devices can utilize photovoltaic effect to leverage solar energy to power themselves when the sunlight is sufficient. For IoT devices located inside buildings, no matter at workplace or at home, they actually can be trickle-charged spontaneously, as long as the interior environment has good illumination. Yue *et al.* [68] proposed to use indoor photovoltaic energy to power IoT devices.

Besides the ones listed above, many other kinds of ambient energy can also be leveraged to power IoT devices. Multiple kinds of ambient energy could be utilized by

one IoT device. Main existing challenges in ambient energy harvesting for green IoT include 1) ambient energy is not always available because its availability depends on various natural and man-made factors; 2) for the same reason, it is difficult to schedule IoT device functionalities based on the available green energy prediction; 3) the ambient energy harvesting efficiencies of the up-to-date harvesters are not sufficiently high; even though the ambient energy is always present, the instantaneously harvested green energy may still be not sufficient to support the IoT device functionalities;
4) conventional single-battery IoT devices cannot achieve concurrent ambient energy harvesting and IoT functionalities because a single rechargeable battery cannot be charged and discharges simultaneously as electric current flow is directional. Motivated by these challenges, we propose dual-battery green energy harvesting architecture to mitigate these constraints for IoT devices.

4.1.2 Dual-Battery Green Energy Harvesting Architecture for IoT Devices

Here, we propose to adopt dual-battery green energy harvesting architecture for IoT devices. Each IoT device is equipped with dual-battery, ambient energy harvester, energy converter, transceiver and Antenna 1 and 2, as shown in Figure 4.2. Ambient energy harvester is to harvest the ambient energy. One IoT device may leverage multiple kinds of ambient energy, and multiple ambient energy harvesters can be integrated into an IoT device. Energy converter converts the harvested energy into the direct current (DC) to charge battery. Transceiver and Antenna 1 are used to transmit and receive signals. Antenna 2 is used to harvest green RF energy, which will be introduced in Section 4.2.

The dual-battery is operated such that in the current time period (defined as a battery cycle), Battery 1 is to store the harvested ambient energy from the energy harvester and energy converter; at the same time, Battery 2 is discharging energy (the energy was harvested in the previous battery cycle) to power the IoT device. When

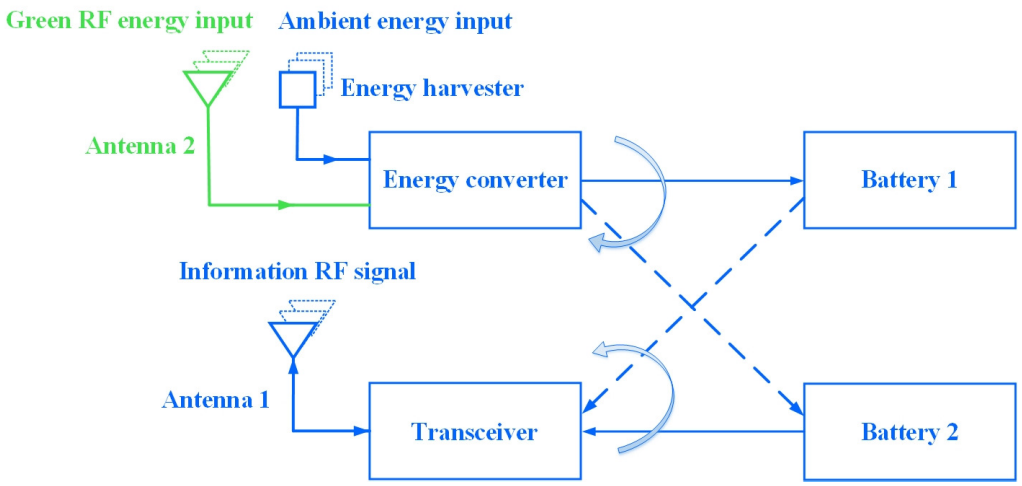

Figure 4.2 Dual-battery green energy harvesting architecture for IoT device.

the next battery cycle begins, Battery 1 starts to discharge its energy (the energy was harvested in the last battery cycle) to power the IoT device. That is, the two batteries alternate their roles of harvesting and discharging in every other battery cycle.

Below are the merits of dual-battery architecture.

1) Dual-battery eliminates the need to predict available ambient energy along the time domain. The amount of harvested ambient energy in the discharging battery is known and accurate. IoT devices can schedule their IoT functionalities along the time domain according to the residual energy in their batteries.

2) Without energy storage, instantaneously harvested ambient energy may not be sufficient to power each individual IoT device; with dual-battery, the harvested ambient energy can be accumulated for a while to reach a certain energy level in the charging battery, and then be utilized to power the IoT device in the next battery cycle.

3) Since a single rechargeable battery cannot be charged and discharges simultaneously, dual-battery facilitates concurrent ambient energy harvesting and

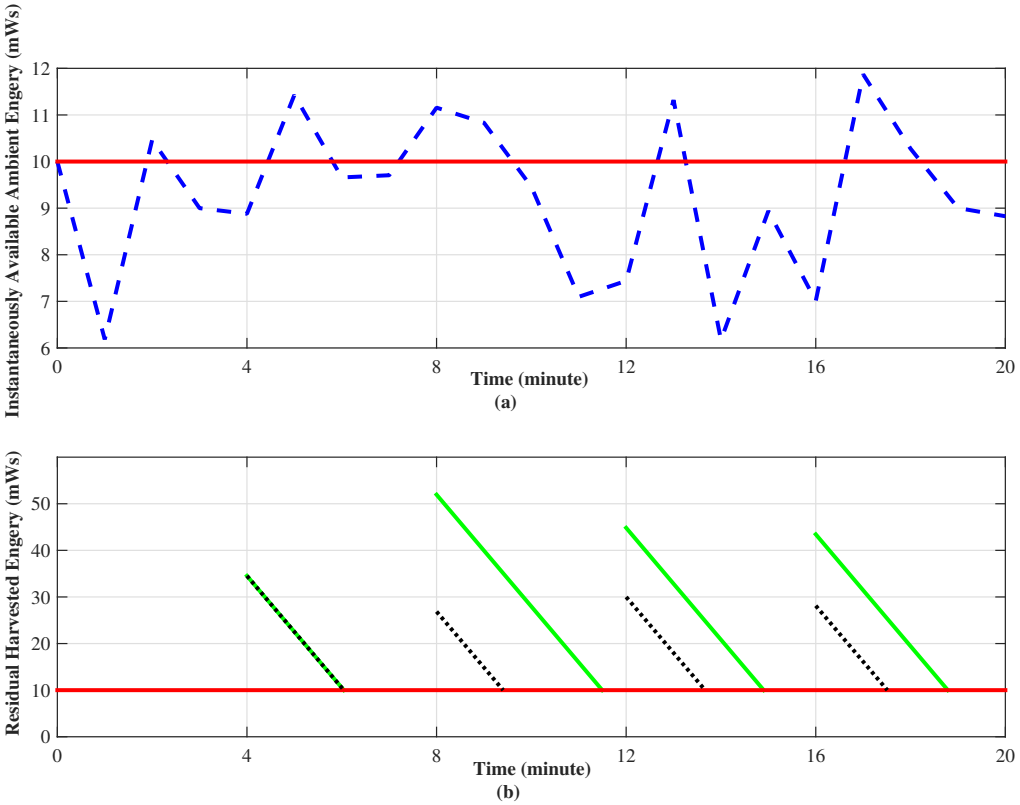

Figure 4.3 Ambient energy distribution and available green energy in different battery scenarios: (a) instantaneous ambient energy distribution; (b) harvested residual green energy for the single-battery scenario vs. dual-battery scenario.

IoT functionalities. There is always one battery harvesting ambient energy, and the other one is discharging to power the IoT device.

We conduct simulations on the ambient energy and the corresponding residual harvested green energy in an IoT device for different battery scenarios in Figure 4.3(a) and Figure 4.3(b), respectively.

Simulations on the instantaneously available ambient energy: The blue-dashed curve in Figure 4.3(a) simulates the instantaneously available ambient energy for an IoT device. The ambient energy is randomly generated between 6mWs and 12mWs along the time axis. Energy loss in converting the instantaneously available ambient energy to power the IoT device is assumed negligible in the simulations. The red-solid curve represents the IoT device's required energy threshold (i.e., 10mWs) for its functionalities. Without energy storage, the IoT device can only perform functionalities when the amount of instantaneously available ambient energy is larger than the IoT device's energy threshold (i.e., the blue curve is above the red curve). In this case, as shown in Figure 4.3(a), the duration of the IoT device that can effectively perform IoT functionalities along the time domain is rather limited.

Simulations on the corresponding residual harvested green energy in different battery scenarios: In Figure 4.3(b), the black-dashed curve stands for the residual harvested energy during the discharging mode in the conventional single-battery scenario. In the first battery cycle (each battery cycle lasts 4 minutes), the IoT device harvests the ambient energy (which is generated as shown in Figure 4.3(a)). In Figure 4.3(b), when the second battery cycle begins, the single-battery starts to discharge electricity to power the IoT device. If the residual green energy in the battery is less than the energy threshold (10 mWs), the single-battery switches to the charging mode to harvest ambient energy, and discharges in the next battery cycle, and so on. The green-solid curve refers to the residual harvested energy during the discharging mode in the dual-battery scenario, in which the IoT device is equipped

with dual-battery. To execute the same IoT functionality, the two scenarios (with single- and dual-battery) perform the same in the second battery cycle because they harvest the same amount of ambient energy in the first battery cycle. In Figure 4.3(b), the single-battery's total harvested green energy is less than that of dual-battery at the beginning of the third battery cycle because the single-battery first spends some time to power IoT device in the second battery cycle, i.e., the single-battery's ambient energy harvesting (recharging) time is less than a full battery cycle. In contrast, the dual-battery has two batteries which can alternately power the IoT device and harvest ambient energy; there is always a battery to harvest ambient energy from the beginning to the end of each battery cycle. The same phenomenon can be observed in subsequent battery cycles.

The key challenges and research directions in realizing dual-battery architecture include: 1) since two batteries are embedded in one IoT device, batteries with large capacity but small size are desired; 2) properly defining battery capacity and battery cycle is critical to maximize the ambient energy utilization; 3) high charging and discharging efficiencies and long lifetime batteries require further research; 4) in order to leverage as many kinds of ambient energy as possible, multiple kinds of energy harvesters may be integrated into one IoT device, and hence the miniaturization of energy harvesters is another key challenge.

4.2 Green Energy Wireless Charging

Wireless charging was not widely adopted in past decades because of both low charging efficiency and brown energy source; tremendous brown energy is consumed at the transmitter but little can be harvested by the receiver [57]. Here, we propose to utilize green energy to wirelessly power IoT devices (even though the wireless charging efficiency is not relatively high, the BSs can keep emitting RF energy for a long time to charge the surrounding IoT devices and the energy sources are green)

and also highlight the latest technological breakthroughs to enhance the efficiency of wireless charging. If the ambient energy sources in the first step are not often present or the ambient energy harvesting rate is too low, the IoT devices will request nearby green BSs for energy replenishment. The nearby green BSs will then emit green RF energy to wirelessly power the IoT devices. Besides other ambient energy harvesters, an IoT device is equipped with Antenna 2 to receive green RF energy, i.e., green color antenna, as shown in Figure 4.2. The green RF energy can be transmitted upon one or multiple public dedicated wireless charging spectrum bands, and thus Antenna 2 can be a single band antenna or multi-band antenna.

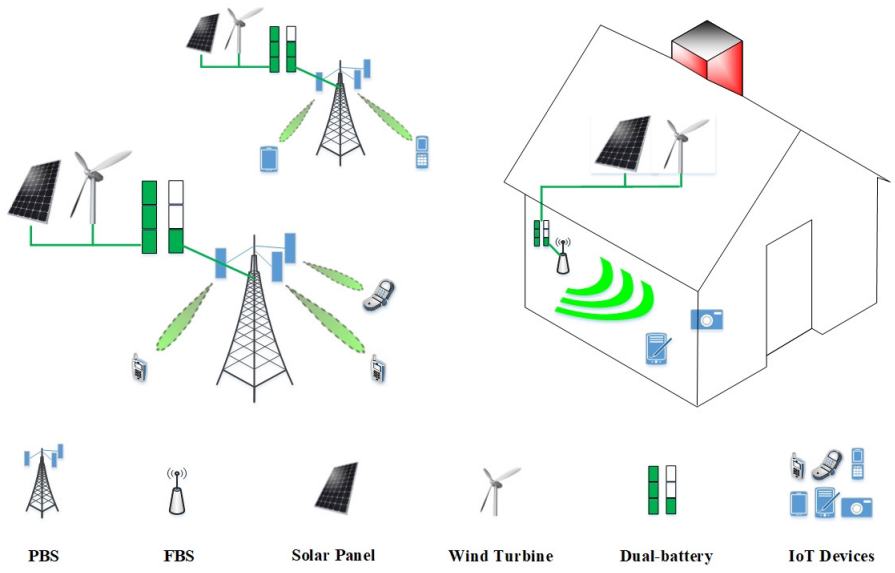

Figure 4.4 Green energy wireless charging architecture.

The green FBSs can be deployed in the indoor environment and equipped with their own dual-batteries, as shown on the right side of Figure 4.4. WiFi access points or Low Power Wide Area (LPWA) transmitters can also be modified and adopted as green FBSs. Via an electric cable, the dual-battery is connected to the solar panel and wind turbine mounted on the roof or exterior wall of a building. As shown on the left side of Figure 4.4, in the outdoor environment, the cellular PBSs are equipped with dual-batteries and powered by green energy as well. Considerable green energy

can be harvested via either a solar panel or wind turbine [48]. Note that solar and wind energy complement each other well in powering the BSs, both on daily and seasonal timescales [48]. The operation of dual-battery at BS is the same as that of aforementioned IoT devices. Benefits of equipping IoT devices with dual-battery are also applicable to equipping green BSs with dual-battery.

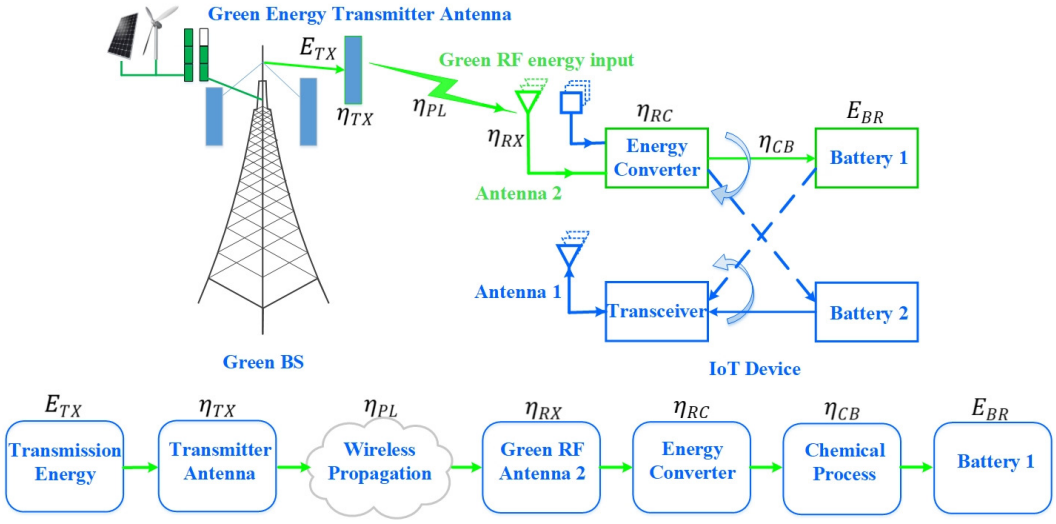

Figure 4.5 Green energy wireless charging efficiency.

When a BS wirelessly transfers green energy to charge an IoT device, as shown in Figure 4.5, the actual energy received by the IoT device's battery can be expressed as

$$E_{BR} = E_{TX} \cdot \eta_{TX} \cdot \eta_{PL} \cdot \eta_{RX} \cdot \eta_{RC} \cdot \eta_{CB}. \tag{4.1}$$

Here, E_{BR} is the amount of energy received at the IoT device's battery. E_{TX} is the amount of green energy wirelessly transmitted by the BS. η_{TX} is the transmitter antenna efficiency, which describes how efficiently the antenna converts transmission power into radio waves headed in a specified direction. η_{PL} is the wireless transfer efficiency due to wireless propagation. η_{RX} is the receiver antenna efficiency, which describes how efficiently the receiver antenna converts radio waves arrived from a

specified direction into alternating current (AC) electrical power. η_{RC} is the energy efficiency of the IoT device's circuit for converting the received AC to the battery-like DC. η_{CB} is the energy efficiency of storing energy into the battery. Thus, the end-to-end green energy wireless charging efficiency is $\frac{E_{BR}}{E_{TX}}$; achieving high end-to-end efficiency is the ultimate goal in wireless charging. The low end-to-end efficiency is the major barrier in past decades for actualizing wireless charging. In Equation 4.1, we can see several terms (factors) that impact the effective green energy received by a battery. In this section, a number of the latest breakthroughs in wireless technologies that can essentially improve green energy wireless charging efficiency are delineated.

4.2.1 Antenna Array and MIMO

A key concern for wireless charging is the attenuation of energy being transferred over a long transmission distance. This issue is especially severe for a single-antenna transmitter. A radical approach to enhance wireless charging efficiency is to deploy multiple antennas at the transmitter and receiver, resulting in a multiple-input and multiple-output (MIMO) system. Antenna array at the green PBSs can focus energy onto small regions of space to yield a large gain. FBSs can also adopt multiple antennas (if the size of antennas can be accommodated in a particular manner). It has been reported in [33] that massive MIMO can enhance the wireless energy transfer efficiency by 100 times; thus, η_{TX} and η_{RX} in Equation 4.1 will be effectively improved. This exceptional energy efficiency has made MIMO one of the promising technologies for wireless energy transfer. Therefore, as shown in Figure 4.2, multiple antennas at Antenna 2 are desired for IoT devices.

Owing to the limitation of the size and weight, some IoT devices may not be able to be equipped with multiple antennas for receiving green RF energy. Multiple-input and single-output (MISO) does not perform as well as MIMO, but still outperforms single-input and single-output (SISO). Miniaturization of antennas

in terms of size and weight at both wireless transmitter and IoT device sides requires further investigation.

4.2.2 Beamforming and Localization

Beamforming can be employed in antenna array and MIMO to improve the efficiency of wireless charging. Multiple antennas collaboratively concentrate green RF energy to a desired direction toward the target IoT device to enhance η_{TX} in Equation 4.1. By radiating the same amount of green RF energy, omni-directional broadcast leads to the lowest wireless charging efficiency; when a number of IoT devices located at the same direction request energy replenishment at the same time, directional green RF beam achieves higher wireless charging efficiency.

In this context, the green BSs should first be aware of the locations of the target IoT devices, and the green RF beams can then be directed toward them. IoT devices with self-localization capability can send their location information to the green BSs with their green energy replenishment requests. IoT devices can also be localized by green BSs. In order to enhance the accuracy of localization, multiple BSs may cooperate to localize IoT devices based on the strength or the time difference of arrivals of the received request signals. For a dynamically changing environment with non-line-of-sight and multi-path propagation, multiple fingerprints of the received request signals may be leveraged to localize the IoT devices [19]. Accurate localization is desirable because the beamforming direction highly depends on the accuracy of each IoT device's localization.

4.2.3 Millimeter-Wave

Millimeter-wave (mm-Wave) (30GHz-300GHz) is a promising candidate for wireless charging. First, mm-Wave systems typically adopt the directed beams, which can exploit directivity gains to improve η_{TX} and η_{RX} in Equation 4.1. Second, the antenna

size is smaller than those of the lower frequency techniques because of the shorter wavelength. Thus, a large number of antennas can be easily deployed in an mm-Wave system at green FBSs and PBSs to serve IoT devices. Also, multiple antennas can be easily integrated into an IoT device, due to small antenna sizes, to realize MIMO (instead of MISO). Third, mm-Wave PBSs are expected to be densely deployed for next generation communications. The distance between an IoT device and the serving green PBS/FBS is expected to be shortened, thus decreasing the wireless propagation path loss, i.e., increasing η_{PL} in Equation 4.1. Fourth, since mm-Wave energy transfer operates in higher frequencies, it has little impact on the existing cellular transmissions. However, the diffusion by rain on mm-Wave is more severe than on other microwave frequencies.

4.2.4 IoT Device Circuit Design and Battery Design

There are two crucial aspects in the IoT device circuit design. The first is impedance matching, which is to reduce the electrical transmission loss from an antenna to a rectifier circuit [46]. A matching circuit is made with reactive component, e.g., capacitors and coils. Maximum energy conversion is realized when the impedance at the antenna and that at the load are conjugate of each other [46]. The second aspect is to design a rectifier, which converts the green RF input captured by antenna into DC voltage; it is usually made with diodes, a diode bridge and a voltage rectifier multiplier. It is challenging to generate a battery-like voltage from low input green RF power in the rectifier. The aforementioned two aspects can enhance the energy conversion efficiency in the circuit of an IoT device, i.e., η_{RC} in Equation 4.1. The state-of-art energy conversion efficiency from an IoT device's receiving antenna to the battery can reach 80% [57]. However, there is still room for further improvement.

Some electrical energy will be lost due to the battery chemical process. The higher charging efficiency of a battery, i.e., η_{CB}, the more converted DC can be

stored into the battery of an IoT device. As aforementioned, achieving high charging efficiency, small size, large capacity and long lifetime battery is the key challenge and the goal of future battery research.

4.2.5 SWIPT

The simultaneous wireless information and power transfer (SWIPT) is another attractive technology. Theoretically, RF information reception and energy harvesting can be performed from the same RF signal input because RF signal carries both information and energy. It is ideal if the IoT devices can be self-powered by receiving data. However, information cannot be readily decoded from the current state-of-the-art energy harvester because information embedded in received signals is lost during the energy harvesting process; inversely, current circuit designs are not yet able to absorb RF energy directly from the decoded information carrier [46]. Advanced entropy retrieval methods deserve further exploration to decode information from the energy harvester [64].

Our proposed dual-battery green energy harvesting architecture achieves SWIPT. As shown in Figure 4.2, Antenna 1 connected with the transceiver is for information transmission and reception, and Antenna 2 equipped with the energy converter is to harvest energy from the RF information signal, thus enabling SWIPT.

4.3 Green Energy Balancing

In the second step, the BSs wirelessly transfer green energy to power the IoT devices. Different BSs may receive different numbers of requests and the required energy replenishment time may also be different, and thus the green energy consumption at each BS varies. The harvested green energy at each BS exhibits temporal and spatial diversities as well. Hence, some of the green BSs may have abundant harvested green energy but serve few IoT devices, while some of them need to power a substantial

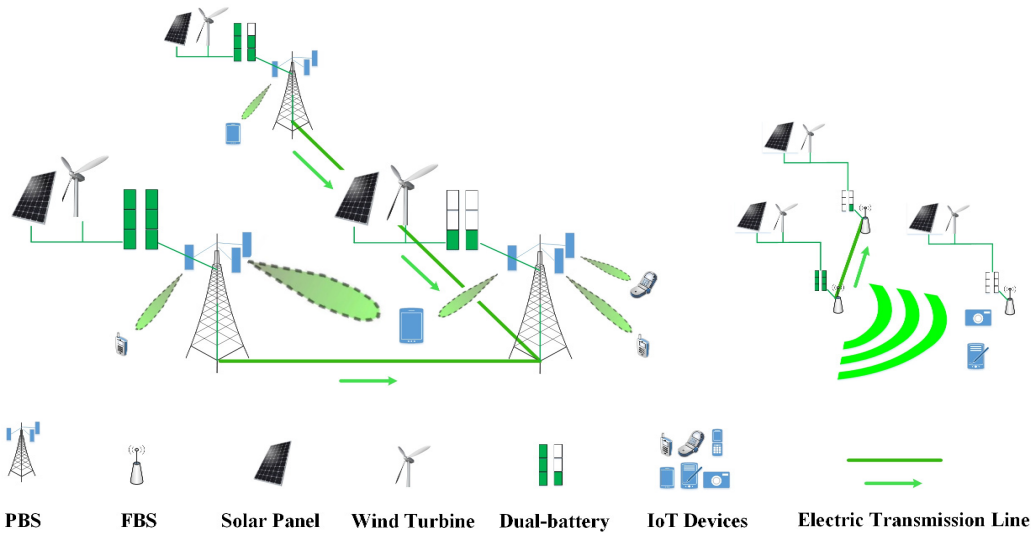

Figure 4.6 Cooperative green energy transfer and wired green energy balancing.

number of surrounding IoT devices but have little residual green energy. The IoT devices in the latter case will lose their opportunities to tap on the main green energy sources. Therefore, in order to further ensure the green energy availability, cooperative wireless green energy transfer and wired green energy balancing are proposed.

4.3.1 Cooperative Green Energy Wireless Charging

As mentioned earlier, some green BSs may not have sufficient green energy to power their surrounding IoT devices. Before this happens, they can seek help from adjacent green BSs. If the adjacent green BSs have abundant green energy, they can cooperatively wirelessly transfer green energy toward the target IoT devices, as shown in Figure 4.6.

The drawback of cooperative wireless green energy transfer is that the adjacent green BSs will consume more green energy to power the IoT devices which are further away because of the severe wireless attenuation. Therefore, advanced cooperative

wireless green energy transfer optimization is needed. It is essential and challenging to determine which green BSs should participate in the cooperative wireless green energy transfer, for how much time, toward which direction and by which level of transmission power. In considering the safety for humans and other living things being exposed to RF waves, sophisticated techniques for channel estimation, power control and adaptive beamforming should be adopted to ensure safety in cooperative green energy transfer.

4.3.2 Wired Green Energy Balancing

Wired green energy balancing is another approach to alleviate the mismatch between the harvested green energy and that to be wirelessly transferred. The green BSs with abundant green energy can transfer green energy to those with insufficient green energy via the electric transmission lines, to supplement their green energy shortages, as shown in Figure 4.6.

The electricity transmission efficiency of electric transmission lines is not 100%; some electrical energy is lost as heat when the electricity traverses the electric transmission lines. The electricity transmission efficiency depends on the distance and material of the electric transmission line between the two BSs. The rationale of this approach is to transfer more electricity through the electric transmission lines with high electricity transmission efficiency among the BSs.

In this approach, the key challenge is to determine which green BSs should transmit to which green BSs by how much electricity to achieve the goal of fulfilling the green energy requirement while minimizing the overall electricity loss during the electricity transmissions. Liu and Ansari [39] proposed to classify the local green BSs into two sets: ***Set* 1** includes the green BSs with insufficient green energy and ***Set* 2** includes those with sufficient green energy. For each time period, the green PBSs in ***Set* 2** transmit electricity to those in ***Set* 1**. According to the different

electricity transmission efficiencies of different electric transmission lines, they have minimized the total electricity transmission loss while alleviating the green energy shortages for the BSs in ***Set* 1**. In their solution, single-hop wired electricity (green energy) transmission is considered, i.e., electricity is directly transmitted from the BSs in ***Set* 2** to those in ***Set* 1**. Some finer electricity transmission schemes, i.e., multiple-hop green energy transmission, may worth further investigation to achieve higher wired electricity transmission efficiency for balancing green energy among BSs. Furthermore, joint optimization of cooperative green energy transfer and wired green energy balancing is another important future research direction.

4.4 Summary

A three-step green IoT architecture has been proposed: 1) IoT devices can harvest ambient energy to be self-powered, in which we have proposed to adopt dual-battery green energy harvesting architecture for powering IoT devices; 2) green BSs intentionally emit RF energy to wirelessly charge the surrounding IoT devices, in which advanced techniques for improving the end-to-end wireless charging efficiency are elaborated; 3) cooperative green energy wireless charging and wired green energy balancing are considered to mitigate the mismatch between the harvested green energy and that to be wirelessly transferred to individual BSs. The latter step reinforces the former one to ensure the green energy availability for IoT devices.

CHAPTER 5

FUTURE WORK

There are mainly three approaches to enhance the green energy utilization in green cellular networks. The first one is mobile user association, the second one is wired green energy transfer, and the third is joint mobile user association and wired green energy transfer. In the first approach, the intuition is to "balance" the communication workloads among BSs to alleviate the mismatch between the available green energy and communication workload demanded energy to achieve a higher green energy utilization. In the second approach, instead of "moving" mobile users among the BSs, we intend to transfer green energy via electric transmission line to "balance" the green energy among the BSs. Our previous works focus on the first approach. Therefore, the future works will focus on the second and third approaches. The performance comparisons among these three approaches will be conducted to achieve the highest green energy utilization. Since many other ICT technologies can be powered by green energy, we also plan to apply dual-battery mechanism to the researches of green data center and green cloudlets.

In addition, the research on green energy wireless charging will be completed in the future. As aforementioned, a number of advancing technologies can further improve the efficiency of wireless charging. We plan to first complete the analytical research in wireless charging. Secondly, We will build the test-bed and implement the prototype of short range wireless charging. Eventually, We will realize the high efficiency green energy wireless charging for mobile IoT devices.

CHAPTER 6

CONCLUSION

In this dissertation, we have proposed and investigated the dual-battery enabled profit driven user association scheme to maximize the profit for network providers in green heterogeneous cellular networks. Unlike most existing green energy related works, there is no need to predict the available green energy; in our work, by equipping dual-battery, the amounts of available green energy at BSs for each time period are known and accurate. We provision a novel pricing model to incentivize network provider to provision lower traffic delivery latency and to gain fairness among mobile users. According to the pricing model and the residual green energy traffic latency ratio, our proposed PDU heuristic algorithm jointly considers the utilization of green energy and traffic delivery latency to associate more mobile users to the BSs with higher residual green energy to traffic latency ratio. We have validated the performance of the proposed algorithm through extensive simulations, and the proposed user association methodology maximizes the profit for the network providers.

Furthermore, in order to facilitate green D2D communications for IoT, we have proposed a novel architecture by adopting the overlay spectrum sharing approach and green relay BSs in heterogeneous cellular networks. In each macrocell, by optimizing the network resource allocation, the required data rates of the SD pairs of IoT applications have been satisfied and all the relay BSs' overall communication energy consumption is minimized. By equipping dual batteries at each relay BS, unlike most existing green energy related works, we do not need to predict the available green energy. The amount of available green energy at a relay BS in each time period is known and accurate. By balancing the residual green energy among the relay BSs, the utilization of green energy has been maximized and the goal of furtherest saving

on-grid energy is achieved. We have validated the performance of the proposed novel architecture through extensive simulations.

Moreover, we have proposed green energy solutions to power IoT devices (i.e., green devices). Three steps for greening IoT have been systematically provisioned: 1) IoT devices can harvest ambient energy to be self-powered, in which we have proposed to adopt dual-battery green energy harvesting architecture for powering IoT devices; 2) green BSs (powered by green energy) will intentionally emit RF energy to wirelessly charge the surrounding IoT devices, in which advanced techniques for improving the end-to-end wireless charging efficiency are elaborated; 3) cooperative green energy wireless charging and wired green energy balancing are considered to mitigate the mismatch between the harvested green energy and that to be wirelessly transferred for individual BSs. The latter step reinforces the former one to ensure the green energy availability for IoT devices. We have also identified the corresponding key challenges as future research directions in line with the three steps. This dissertation will hopefully foster readers for further research to realize green IoT.

BIBLIOGRAPHY

[1] 5G spectrum, Louisville, KY, 2015. [Online]. Available: http://www.gsma.com/spectrum/wp-content/uploads/2015/04/5G-Spectrum-Policy-Position-FINAL.pdf. Accessed on April, 2019.

[2] Digital mobile radio towards future generation systems: Cost 231 final report. Winlab, Rutgers University, New Brunswick, NJ, 1999. [Online]. Available: http://www.winlab.rutgers.edu/~andrej/research/docs/cost231/cover.pdf. Accessed on April, 2019.

[3] Fact sheet: spectrum frontiers rules identify, open up vast amount of new high-band spectrum for next generation (5g) wilress broadband. Federal Communications Commission, Washington, DC, 2016. [Online]. Available: http://apps.fcc.gov/edocs_public/attachmatch/DOC-340310A1.pdf. Accessed on April, 2019.

[4] Low throughput networks: Use case, functional architecture, and protocols. Group Specification Low Throughput Networks 001. Sophia Antipolis Cedex, France, 2014. [Online]. Available: https://www.etsi.org/deliver/etsi_gs/ltn/001_099/002/01.01.01_60/gs_ltn002v010101p.pdf. Accessed on April, 2019.

[5] Sustainable energy use in mobile communications. Ericsson, New York City, NY, 2007. [Online]. Available: https://www.scirp.org/(S(351jmbntvnsjt1aadkposzje))/reference/ReferencesPapers.aspx?ReferenceID=998346&btwaf=12322209. Accessed on April, 2019.

[6] J. Andrews et al. An overview of load balancing in hetnets: Old myths and open problems. *IEEE Wireless Communications*, 21(2):18–25, 2014.

[7] J. Andrews et al. What will 5G be? *IEEE Journal on Selected Areas in Communications*, 32(6):1065–1082, 2014.

[8] N. Ansari and T. Han. *Green Mobile Networks: A Networking Perspective*. New York City, NY: Wiley-IEEE Press, 2017.

[9] E. Aryafar et al. RAT selection games in HetNets. *IEEE International Conference on Computer Communications (INFOCOM)*, pages 998–1006, 2013.

[10] G. Auer et al. How much energy is needed to run a wireless network? *IEEE Wireless Communications*, 18(5):40–49, 2011.

[11] S. Borst et al. Dynamic optimization in future cellular networks. *Bell Labs Technical Journal*, 10(2):99–119, 2005.

[12] S. Boyd and L. Vandenberghe. *Convex optimization*. New York City, NY: Cambridge University Press, 2004.

[13] V. Chamola, B. Krishnamachari, and B. Sikdar. Green energy and delay aware downlink power control and user association for off-grid solar-powered base stations. *IEEE Systems Journal*, 12(3):2622–2633, 2018.

[14] S. Corroy, L. Falconetti, and R. Mathar. Dynamic cell association for downlink sum rate maximization in multi-cell heterogeneous networks. *IEEE International Conference on Communications (ICC)*, Feb. 2012.

[15] A. Damnjanovic et al. A survey on 3GPP heterogeneous networks. *IEEE Wireless Communications*, 18(3):10–21, 2011.

[16] M. Garey and S. D. Johnson. *Computer and Intractability: A Guide to the Theory of NP-completeness*. New York City, NY: W. H. Freeman and Company, 1979.

[17] X. Ge et al. 5G ultra-dense cellular networks. *IEEE Wireless Communications*, 23(1):72–79, 2016.

[18] M. Gorlatova et al. Movers and shakers: Kinetic energy harvesting for the internet of things. *IEEE Journal on Selected Areas in Communications*, 33(8):1624–1639, 2015.

[19] X. Guo, L. Chu, and X. Sun. Accurate localization of multiple sources using semidefinite programming based on incomplete range matrix. *IEEE Sensors Journal*, 16(13):5319–5324.

[20] T. Han and N. Ansari. ICE: Intelligent cell breathing to optimize the utilization of green energy. *IEEE Communications Letters*, 16(6):866–869, 2012.

[21] T. Han and N. Ansari. Heuristic relay assignments for green relay assisted device to device communications. *IEEE Global Communications Conference (GLOBECOM)*, pages 468–473, 2013.

[22] T. Han and N. Ansari. On optimizing green energy utilization for cellular networks with hybrid energy supplies. *IEEE Transactions on Wireless Communication*, 12(8):3872–3882, 2013.

[23] T. Han and N. Ansari. Powering mobile networks with green energy. *IEEE Wireless Communications*, 21(1):90–96, 2014.

[24] T. Han and N. Ansari. A traffic load balancing framework for software-defined radio access networks powered by hybrid energy sources. *IEEE/ACM Transactions on Networking*, 24(2):1038–1051, 2016.

[25] T. Han and N. Ansari. Network utility aware traffic load balancing in backhaul-constrained cache-enabled small cell networks with hybrid power supplies. *IEEE Transactions on Mobile Computing*, 16(10):2819–2832, 2017.

[26] Z. Hasan, H. Boostanimehr, and V. Bhargava. Green cellular networks: A survey, some research issues and challenges. *IEEE Communications Surveys and Tutorials*, 13(4):524–540, Fourth Quarter 2011.

[27] X. Huang, T. Han, and N. Ansari. On green energy powered cognitive radio networks. *IEEE Communications Surveys and Tutorials*, 17(2):827–842, Second Quarter, 2015.

[28] X. Huang, T. Han, and N. Ansari. Smart grid enabled mobile networks: Jointly optimizing BS operation and power distribution. *IEEE/ACM Transactions on Networking*, 25(3):1832–1845, 2017.

[29] H.-S. Jo et al. Heterogeneous cellular networks with flexible cell association: A comprehensive downlink SINR analysis. *IEEE Transactions on Wireless Communications*, 11(10):3484–3495, Oct. 2012.

[30] A. Kiani and N. Ansari. Profit maximization for geographical dispersed green data centers. *IEEE Transactions on Smart Grid*, 9(2):703–711, 2016.

[31] H. Kim et al. Distributed α-optimal user association and cell load balancing in wireless networks. *IEEE/ACM Transactions on Networking*, 20(1):177–190, 2012.

[32] L. Kleinrock. *Queueing Systems, Volume 2: Computer Applications*. New York City, NY: Wiley New York, 1976.

[33] E. Larsson et al. Massive MIMO for next generation wireless systems. *arXiv preprint arXiv:1304.6690*, 2013.

[34] X. Lin, J. Andrews, and A. Ghosh. Spectrum sharing for device-to-device communication in cellular networks. *IEEE Transactions on Wireless Communications*, 13(12):6727–6740, 2014.

[35] X. Lin et al. An overview of 3GPP device-to-device proximity services. *IEEE Communications Magazine*, 52(4):40–48, 2014.

[36] J. Liu et al. Device-to-device communication in LTE-advanced networks: a survey. *IEEE Communications Surveys and Tutorials*, 17(4):1923–1940, 2014.

[37] J. Liu et al. Device-to-device communications achieve efficient load balancing in LTE - advanced networks. *IEEE Wireless Communications*, 21(2):57–65, 2014.

[38] X. Liu and N. Ansari. Green relay assisted D2D communications with dual battery for IoT. *IEEE Global Communications Conference (GLOBECOM)*, pages 1–6, 2016.

[39] X. Liu and N. Ansari. Green relay assisted D2D communications with dual batteries in heterogeneous cellular networks for IoT. *IEEE Internet of Things Journal*, 4(5):1707–1715, 2017.

[40] X. Liu and N. Ansari. Profit driven user association with dual batteries in green heterogeneous cellular networks. *IEEE Global Communications Conference (GLOBECOM)*, pages 1–6, 2017.

[41] X. Liu and N. Ansari. Dual-battery enabled profit driven user association in green heterogeneous cellular networks. *IEEE Transactions on Green Communications and Networking*, 2(4):1002–1011, 2018.

[42] X. Liu and N. Ansari. Toward green iot: Energy solutions and key challenges. *IEEE Communications Magazine*, 57(3):104–110, 2019.

[43] X. Liu, T. Han, and N. Ansari. Intelligent battery management for cellular networks with hybrid energy supplies. *IEEE Wireless Communications and Networking Conference (WCNC)*, pages 1–6, Apr. 2016.

[44] X. Liu, X. Huang, and N. Ansari. Green energy driven user association in cellular networks with dual battery system. *IEEE International Conference on Communications (ICC)*, pages 1–6, 2016.

[45] D. Lopez-Perez et al. Enhanced intercell interference coordination challenges in heterogeneous networks. *IEEE Wireless Communications*, 18(3):22–30, 2011.

[46] X. Lu et al. Wireless networks with rf energy harvesting: A contemporary survey. *IEEE Communications Surveys and Tutorials*, 17(2):757–789, 2015.

[47] S. Luo, R. Zhang, and T. Lim. Optimal save-then-transmit protocol for energy harvesting wireless transmitters. *IEEE Transactions on Wireless Communications*, 12(3):1196–1207, 2013.

[48] Y. Mao et al. Energy harvesting small cell networks: feasibility, deployment, and operation. *IEEE Communications Magazine*, 53(6):94–101, 2015.

[49] F. Martin et al. Energy efficiency of the internet of things. *Technology and Energy Assessment Report prepared for IEA 4E EDNA*, 2016.

[50] B. Negra, J. Todorovic, and T. Ackermann. Loss evaluation of HVAC and HVDC transmission solutions for large offshore wind farms. *Electric Power Systems Research*, 76(11):916–927, 2006.

[51] E. Oh et al. Toward dynamic energy-efficient operation of cellular network infrastructure. *IEEE Communications Magazine*, 49(6), 2011.

[52] M. Palattella et al. Internet of things in the 5G era: Enablers, architecture, and business models. *IEEE Journal on Selected Areas in Communications*, 34(3):510–527, 2016.

[53] B. Ren et al. Cellular communications on license-exempt spectrum. *IEEE Communications Magazine*, 54(5):146–153, 2016.

[54] F. Richard. *The Feynman Lectures on Physics Vol I.* Boston, MA: Addison Wesley, 1970.

[55] F. Shaikh, S. Zeadally, and E. Exposito. Enabling technologies for green internet of things. *IEEE Systems Journal*, 11(2):983–994, 2017.

[56] C. E. Shannon. *The Mathematical Theory of Communication.* Champaign, IL: University of Illinois Press, 2002.

[57] N. Shinohara. *Wireless Power Transfer via Radiowaves.* Hoboken, NJ: Wiley Press, 2013.

[58] S. Singh, H. S Dhillon, and J. Andrews. Offloading in heterogeneous networks: Modeling, analysis, and design insights. *IEEE Transactions on Wireless Communications*, 12(5):2484–2497, 2013.

[59] H. Tam et al. Joint load balancing and interference management for small-cell heterogeneous networks with limited backhaul capacity. *IEEE Transactions on Wireless Communications*, 16(2):872–884, 2017.

[60] M. Tehrani, M. Uysal, and H. Yanikomeroglu. Device-to-device communication in 5G cellular networks: challenges, solutions, and future directions. *IEEE Communications Magazine*, 52(5):86–92, 2014.

[61] Q. Wan et al. Analysis and design of a thermoelectric energy harvesting system with reconfigurable array of thermoelectric generators for iot applications. *IEEE Transactions on Circuits and Systems I: Regular Papers*, 64(9):2346–2358, 2017.

[62] B. Wang et al. Resource allocation optimization for device-to-device communication underlaying cellular networks. *IEEE 73rd Vehicular Technology Conference (VTC)*, pages 1–6, 2011.

[63] F. Wang et al. Energy-efficient resource allocation for device-to-device underlay communication. *IEEE Transactions on Wireless Communications*, 14(4):2082–2092, 2015.

[64] H. Wu et al. Joint entropy based learning model for image retrieval. *Journal of Visual Communication and Image Representation*, 55(1):415–423, 2018.

[65] Y. Wu et al. Device-to-device meets LTE-unlicensed. *IEEE Communications Magazine*, 54(5):154–159, 2016.

[66] Q. Ye et al. User association for load balancing in heterogeneous cellular networks. *IEEE Transactions on Wireless Communications*, 12(6):2706–2716, 2013.

[67] C. Yu et al. Resource sharing optimization for device-to-device communication underlaying cellular networks. *IEEE Transactions on Wireless Communications*, 10(8):2752–2763, 2011.

[68] X. Yue et al. Development of an indoor photovoltaic energy harvesting module for autonomous sensors in building air quality applications. *IEEE Internet of Things Journal*, 4(6):2092–2103, 2017.

[69] G. Zhao et al. Power and channel allocation for cooperative relay in cognitive radio networks. *Journal of Selected Topics in Signal Processing*, 5(1):151–159, 2011.

[70] J. Zhou et al. Energy source aware target cell selection and coverage optimization for power saving in cellular networks. *IEEE/ACM International Conference on Green Computing and Communications*, pages 1–8, Dec. 2010.

[71] J. Zhou et al. Energy source aware target cell selection and coverage optimization for power saving in cellular networks. *IEEE/ACM Int'l Conference on Green Computing and Communications & Int'l Conference on Cyber, Physical and Social Computing*, pages 1–8, 2010.